



SARS-CoV-2 Spike Furin Cleavage Site and S2' Basic Residues Modulate the Entry Process in a Host Cell-Dependent Manner

 Muriel Lavie,^a  Jean Dubuisson,^a Sandrine Belouzard^a

^aUniversity of Lille, CNRS, Inserm, CHU Lille, Institut Pasteur de Lille, U1019 - UMR 9017 - CIL - Center for Infection and Immunity of Lille, Lille, France

ABSTRACT SARS-CoV-2 spike (S) envelope glycoprotein constitutes the main determinant of virus entry and the target of host immune response, thus being of great interest for antiviral research. It is constituted of S1 and S2 subunits, which are involved in ACE2 receptor binding and fusion between the viral envelope and host cell membrane, respectively. Induction of the fusion process requires S cleavage at the S1-S2 junction and the S2' site located upstream of the fusion peptide. Interestingly, the SARS-CoV-2 spike harbors a 4-residue insertion at the S1-S2 junction that is absent in its closest relatives and constitutes a polybasic motif recognized by furin-like proteases. In addition, the S2' site is characterized by the presence of conserved basic residues. Here, we sought to determine the importance of the furin cleavage site (FCS) and the S2' basic residues for S-mediated entry functions. We determined the impact of mutations introduced at these sites on S processing, fusogenic activity, and its ability to mediate entry in different cellular backgrounds. Strikingly, mutation phenotypes were highly dependent on the host cell background. We confirmed that although the FCS was not absolutely required for virus entry, it contributed to extending the fusogenic potential of S. Cleavage site mutations, as well as inhibition of furin protease activity, affected the cell surface expression of S in a host cell-dependent manner. Finally, inhibition of furin activity differentially affected SARS-CoV-2 virus infectivity in the tested host cells, thereby confirming the host cell-dependent effect of spike processing for the viral life cycle.

IMPORTANCE SARS-CoV-2 is responsible for the current global pandemic that has resulted in several million deaths. As the key determinant of virus entry into host cells and the main target of host immune response, the spike glycoprotein constitutes an attractive target for therapeutics development. Entry functions of spike rely on its processing at two sites by host cell proteases. While SARS-CoV-2 spike differs from its closest relatives by the insertion of a basic furin cleavage motif at the first site, it harbors conserved basic residues at the second cleavage site. Characterization of the importance of the basic sequences present at the two cleavage sites revealed that they were influencing spike processing, intracellular localization, induction of fusion, and entry in a host cell-dependent manner. Thus, our results revealed a high heterogeneity in spike sequence requirement for entry functions in the different host cells, in agreement with the high adaptability of the SARS-CoV-2 virus.

KEYWORDS coronavirus, SARS-CoV-2, S glycoprotein, viral entry, membrane fusion, host cell

In 2019, the new coronavirus, SARS-CoV-2, which is responsible for the current global pandemic, emerged. Coronaviruses are a diverse family of viruses infecting mammals and birds. Until now, 7 coronaviruses have been shown to infect humans. Four of them (HCoV-229E, HCoV-OC43, HCoV-NL63, and HCoV-HKU1) mainly replicate in the upper respiratory tract and are associated with the mild symptoms of seasonal common colds, while SARS-CoV, MERS-CoV, and SARS-CoV-2, with a zoonotic origin, are responsible for

Editor Tom Gallagher, Loyola University Chicago

Copyright © 2022 American Society for Microbiology. All Rights Reserved.

Address correspondence to Muriel Lavie, muriel.lavie@ibl.cnrs.fr.

The authors declare no conflict of interest.

Received 21 March 2022

Accepted 24 May 2022

Published 9 June 2022

severe, life-threatening respiratory pathologies. Among the structural proteins of SARS-CoV-2 particles, the spike glycoprotein (S) is anchored in the virus envelope and constitutes the main determinant of virus entry. This trimeric type I fusion protein is organized into two subunits. The N-terminal subunit, S1, is responsible for the interaction with the angiotensin-converting enzyme 2 (ACE2) receptor, whereas the C-terminal S2 subunit contains the fusion machinery that mediates the merging between the viral envelope and the cellular membrane. In order to catalyze fusion, S has to be cleaved at the S1 and S2 interface (S1-S2 site) and at the S2' site located upstream from the fusion peptide (reviewed by Tang et al. [1]). These triggering events can be performed by several different proteases such as members of the endosomal cathepsins family, members of the type II transmembrane serine proteases (TTSPs), or furin-like proteases (2, 3). Depending on the type of proteases expressed in the host cell, coronaviruses can follow two distinct entry pathways (1, 4). Thus, in the presence of certain plasma membrane-associated proteases such as the transmembrane protease/serine subfamily member 2 (TMPRSS2), the proteolytic activation of S occurs at the cell surface, which leads to the fusion between the plasma membrane and the viral envelope. This pathway is called the early entry pathway. Conversely, in the absence of such proteases, the viral particle is internalized in the host cell's endosomes, and the fusion is induced upon cathepsin-mediated proteolysis. This pathway is named the late or endosomal entry pathway.

While the presence of 2 basic residues (KR) at the S2' site is conserved between SARS-CoV-2 and SARS-CoV S proteins, SARS-CoV-2 S differs from related coronavirus S proteins by the insertion of 4 residues at the S1-S2 junction. This motif (RRAR) constitutes a polybasic cleavage site that can be targeted by furin-like proteases (5). Such a cleavage site has also notably been found in the more distantly related MERS-CoV. Cellular expression of SARS-CoV-2 S induces fusion of adjacent cells, which leads to the formation of multinucleated syncytia (5–7). Moreover, occurrence of syncytia has been reported in lung tissues of SARS-CoV-2-infected patients (6, 8–11).

Several studies have shown that the deletion of the furin cleavage site (FCS) was detrimental to the propagation of the virus in lung cells as well as in different animal models (5, 12, 13). However, this motif has been shown to be rapidly lost upon passaging of the virus in VeroE6 cells (14–19). Moreover, some FCS-deficient isolates have been reported to occur among infected patients (15, 16). These data underscore how the S protein cleavage site requirement strongly depends on the host cell context.

To further characterize the importance of the FCS and the S2' basic residues for SARS-CoV-2 S protein entry functions, we determined the impact of mutations introduced in these regions (i) on the processing of S, (ii) on its ability to induce syncytia, and (iii) on its ability to mediate entry in different cellular backgrounds in the presence or absence of TMPRSS2. We found that mutations in the FCS affected S functions in a cell type-dependent manner.

RESULTS

SARS-CoV-2 S protein processing is differentially modulated according to S expression context. In a first step to approaching the importance of the SARS-CoV-2 S1-S2 cleavage for the virus life cycle, we compared the different processed forms produced in the context of transfected or infected VeroE6 cells with those associated with SARS-CoV-2 authentic virions or pseudoparticles (Fig. 1, SARS-CoV-2 and SARS2-Spp). Murine leukemia virus retroviral particles pseudotyped with coronavirus S protein (SARS-CoV-2pp) are commonly used to study coronaviruses. To facilitate the identification of the different S species, we included in our analysis the S Δ fur mutant whose S1-S2 site has been replaced by that of the related SARSr-CoV S CZX21 (20), which is devoid of a multibasic cleavage site (Fig. 2A). Interestingly, Western blotting of S species associated with SARS-CoV-2 viral particles and infected VeroE6 cells revealed that the noncleaved form, named S0 (180 kDa), was predominant, while a weaker signal was observed at a lower molecular mass, most probably corresponding to the S2 processed form (100 kDa). Indeed, this product became barely detectable in cells expressing the S Δ fur mutant that lacks the S1-S2 multibasic furin cleavage site (Fig. 1, SARS2-

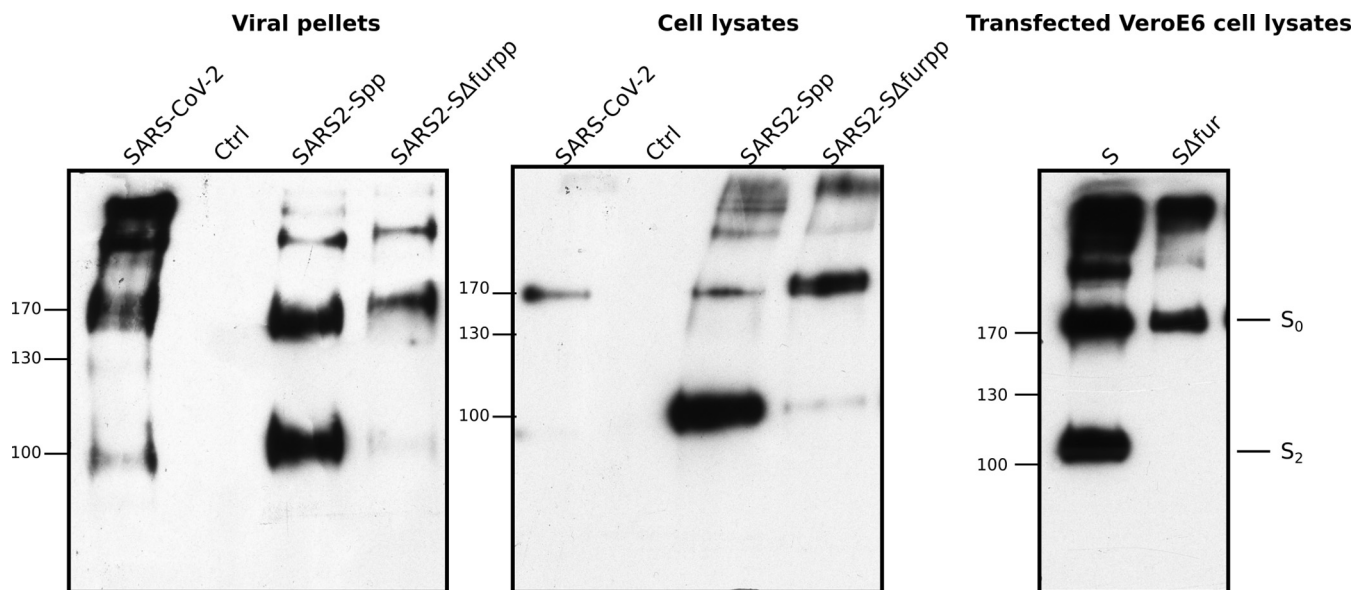


FIG 1 Processing of SARS-CoV-2 spike in different expression contexts. Cell lysates or concentrated supernatants (viral pellets) of SARS-CoV-2-infected VeroE6 cells (SARS-CoV-2, Ctrl), SARS-CoV-2pp retroviral pseudoparticle 293T producer cells (SARS2-Spp, SARS2-S Δ furpp), as well as lysates from S- and S Δ fur-expressing VeroE6 cells, were analyzed by Western blotting using an anti-spike antibody. The positions of molecular weight markers are indicated on the sides of the blots and are expressed in kilodaltons.

S Δ furpp and S Δ fur). In contrast, in S-transfected VeroE6 cell lysates, SARS-CoV-2pp viral pellet, and SARS-CoV-2pp 293T producer cell lysates (Fig. 1, SARS2-Spp), a stronger signal was observed for the processed S₂ form, thus showing that a larger fraction of S was cleaved in this context. These results show that despite the presence of a furin cleavage site, the spike proteins associated with virions secreted by VeroE6 cells are mainly uncleaved, whereas cleaved and uncleaved forms are associated with pseudoparticles. This result suggests that S₁-S₂ processing efficiency is modulated by the cellular context of expression and is in agreement with previous results showing that it is not absolutely required for the virus life cycle (12, 21).

S₂' KR residues are required for TMPRSS2 activation of SARS-CoV-2pp entry, but S₁-S₂ basic residues are dispensable. In order to trigger fusion, the coronavirus S protein has to be cleaved at both the S₁-S₂ and S₂' sites (1). Basic residues located upstream from the fusion peptide of SARS-CoV S (K, R) have been shown to be important for the activation of the fusogenic activity of S by TMPRSS2 (22). With these residues being conserved in SARS-CoV-2 S, we wondered whether they would play a role in S functions. Thus, we first investigated the importance of the FCS and S₂' KR residues for the entry step of the SARS-CoV-2 virus life cycle by producing SARS-CoV-2pp harboring different S mutants. In addition to the S Δ fur mutant, we generated another mutant in the FCS by replacing the first arginine residue (R682) of the furin-like protease cleavage motif with a glutamine residue (S R682Q mutant). This mutation has been reported to arise naturally upon SARS-CoV-2 propagation in VeroE6 cells (14). Furthermore, we mutated S₂' KR residues (K814A and N815N) in the wild-type spike (S_{wt}) and S Δ fur background (Fig. 2A, S S₂', S Δ furS₂'). Of note, the S Δ fur mutant that harbors the SARS-CoV S₁-S₂ sequence still contains a basic residue (R685 in the SARS-CoV-2-S_{wt} sequence corresponding to R667 in the SARS-CoV-1 S_{wt} sequence) at the S₁-S₂ site (Fig. 2A). This residue can be targeted by TMPRSS2 protease and has been shown to modulate the priming of SARS-CoV S protein (22). We thus also evaluated the importance of this residue for the S Δ fur phenotype by mutating it (S Δ furR685N). We first tested the effect of the mutations in FCS and S₂' basic residues on SARS-CoV-2 pseudoparticles infectivity in VeroE6, 293T-ACE2, A549-ACE2, and Huh7-ACE2 cells in the presence or absence of TMPRSS2. Infectivity levels of S Δ fur particles were 10-fold higher than that of S_{wt}pp in VeroE6, 293T-ACE2, and A549-ACE2 cells, while no strong

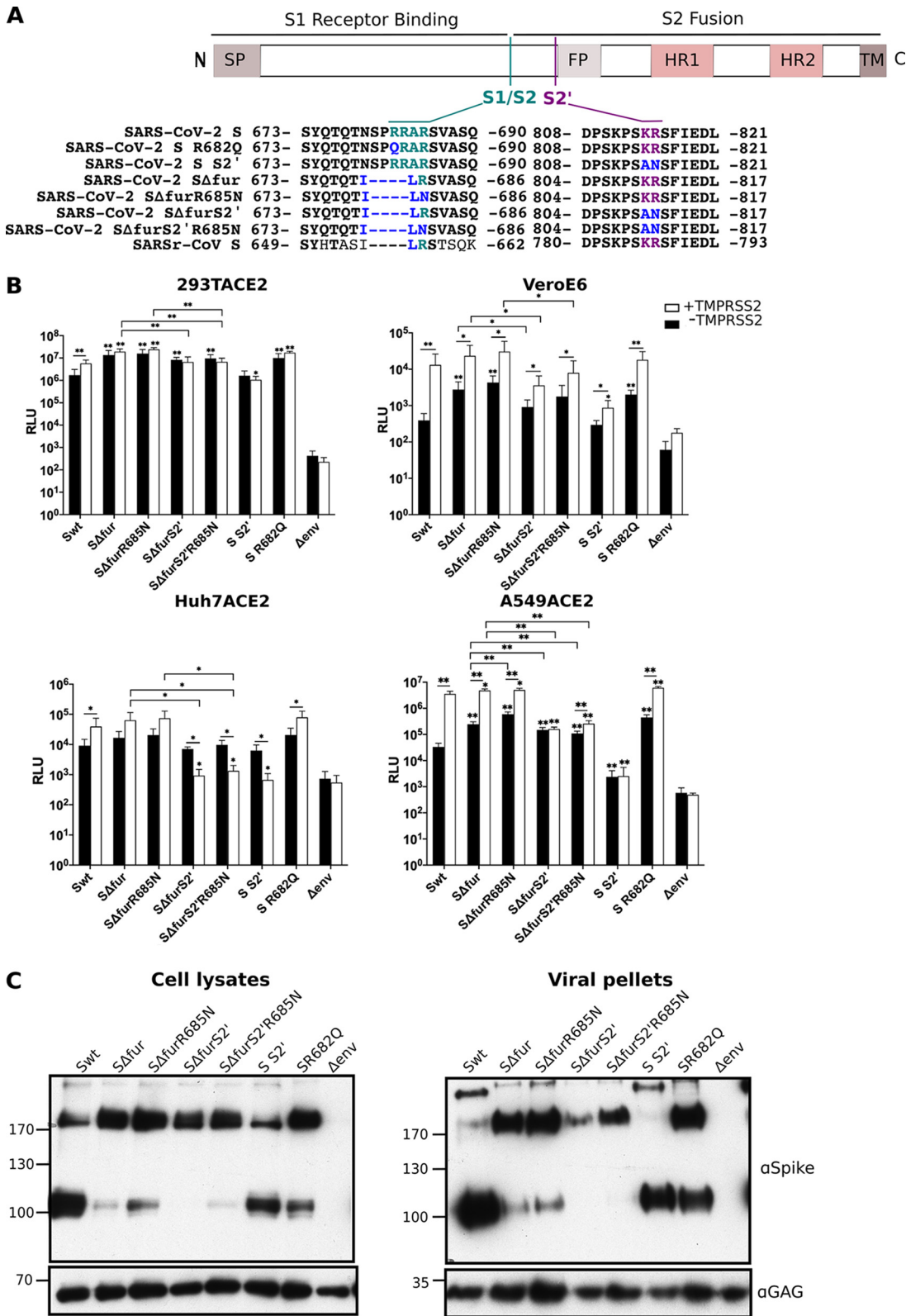


FIG 2 Impact of mutations of FCS and S2' KR residues on SARS-CoV-2pp infectivity. (A) Schematic representation of SARS-CoV-2 spike. The signal peptide (SP), fusion peptide (FP), heptad repeat 1 and 2 (HR1, HR2), and transmembrane (TM) regions are indicated by colored rectangles. The sequence alignment of S1-S2 (blue-green) and S2' cleavage sites (violet) of wild-type and mutant SARS-CoV-2 spike are shown. Multibasic residues constitutive of a furin-like protease cleavage site are shown in blue-green; mutations introduced in this study appear in blue. (B) Infectivity of SARS-CoV-2pp harboring different spike (Continued on next page)

difference was observed in Huh7-ACE2 cells (Fig. 2B). TMPRSS2 expression improved infectivity of most pseudovirions in the four cell lines (Fig. 2, white bars), but the difference between the wild-type (WT) and FCS mutant particles' infectivity in 293T-ACE2, VeroE6, and A549-ACE2 cells was strongly attenuated or abolished upon expression of TMPRSS2 in these cells (Fig. 2, white bars, S Δ fur and S R682Q compared to S). Introduction of the R685N mutation had no additional effect on S Δ furpp infectivity in the different cellular backgrounds expressing TMPRSS2 (Fig. 2B), showing that basic residues at the S1-S2 boundary are dispensable for TMPRSS2-mediated entry. Interestingly, only in A549-ACE2 cells, S2' site KR mutations led to a 14-fold decrease in infectivity level. Moreover, KR mutations strongly attenuated or suppressed TMPRSS2-mediated enhancement of infectivity in VeroE6, 293T-ACE2, and A549-ACE2 cells (Fig. 2B). Surprisingly, in Huh7-ACE2 cells, KR mutants exhibited even lower infectivity levels upon expression of TMPRSS2. We also determined the level of incorporation of the different mutants in retroviral pseudoparticles by Western blotting (Fig. 2C). No striking differences could be observed in the number of incorporated S mutants.

Taken together, these results show that the FCS and S2' KR residues modulate SARS-CoV-2 entry in a cell type-dependent manner. While S2' KR residues are required for TMPRSS2-mediated infection, the S1-S2 basic residues are dispensable for this early entry pathway.

Interestingly, TMPRSS2 has been reported to cleave the C-terminal part of ACE2, resulting in the production of a 13-kDa fragment, and this processing has been shown to be required for enhancing SARS-CoV S-mediated entry (23). In order to check the effect of TMPRSS2 expression on ACE2 in the different cell lines, we characterized the ACE2 migration profile by immunoblotting (Fig. 3A). As shown in Fig. 3A, TMPRSS2 expression affected the migration profile of ACE2 in the four cell lines in different manners. In 293T-ACE2 and Huh7-ACE2 cells, TMPRSS2 expression led to the appearance of products of lower molecular weight that most probably correspond to ACE2 cleavage products, whereas in VeroE6 and A549-ACE2 cells, only a smear of weak intensity could be observed beneath the main band.

These findings suggest that ACE2 is processed differently in the four studied cell lines. Thus, since TMPRSS2 expression was associated with an increase in SARS-CoV-2pp infectivity in the four cell lines, no direct correlation could be drawn between the enhancer effect of TMPRSS2 on infectivity and its ability to cleave ACE2 in our assays.

Deletion of the FCS favors cathepsin-mediated entry pathway. In our pseudoparticle-based infection assays, higher levels of infectivity were observed for the FCS mutants than the WT SARS-CoV-2pp in VeroE6, 293T-ACE2, and A549-ACE2 cells. However, these differences were partly abrogated upon TMPRSS2 expression in these cells. Previous published data have indicated that entry of SARS-CoV-2pp in 293T-ACE2 and VeroE6 cells occurs via the endosomal pathways (4, 12). Thus, this result suggests that FCS mutations provide an advantage for entry via the endosomal pathway only. To test this hypothesis, we inhibited the early or endosomal entry pathway using specific inhibitors of proteases involved in each pathway. Therefore, E64D (aloxistatin) was used to inhibit cathepsins B and L, whose proteolytic activity is required for endosomal entry, whereas camostat mesylate was used to inhibit TMPRSS2 serine protease activity (24) that is required for the early entry pathway (Fig. 4A). E64D treatment inhibited infectivity of Swt and S Δ fur particles in

FIG 2 Legend (Continued)

mutants in VeroE6, 293T-ACE2, A549-ACE2, and Huh7-ACE2 cells transduced or not transduced with TMPRSS2-expressing lentiviruses. Cells were transduced or not transduced with ACE2 (Huh7-ACE2)- or TMPRSS2-expressing lentiviral vectors (Huh7-ACE2-TMPRSS2, VeroE6-TMPRSS2, 293T-ACE2-TMPRSS2, and A549-ACE2-TMPRSS2). Seventy-two to 96 h posttransduction, cells were infected with MLV retroviral particles pseudotyped with WT or mutant SARS-CoV-2 spike. Infectivity was determined by measuring the activity of the luciferase reporter gene in infected cell lysates. Pseudotyped particles produced in the absence of envelope protein were used as negative controls. Results are reported as the means \pm standard deviations (error bars) of at least three independent experiments. Statistics were determined by Mann-Whitney test with multiple comparison to S WT (results shown above the column) or other mutants when specified (*, $P < 0.05$; **, $P < 0.01$; ***, $P < 0.001$). (C) Effect of spike mutations on the incorporation of the envelope proteins in SARS-CoV-2pp. Cell lysates and concentrated supernatants of SARS-CoV-2pp 293T producer cells were analyzed by Western blotting using monoclonal antibodies (MAbs) against spike and MLV capsid protein.

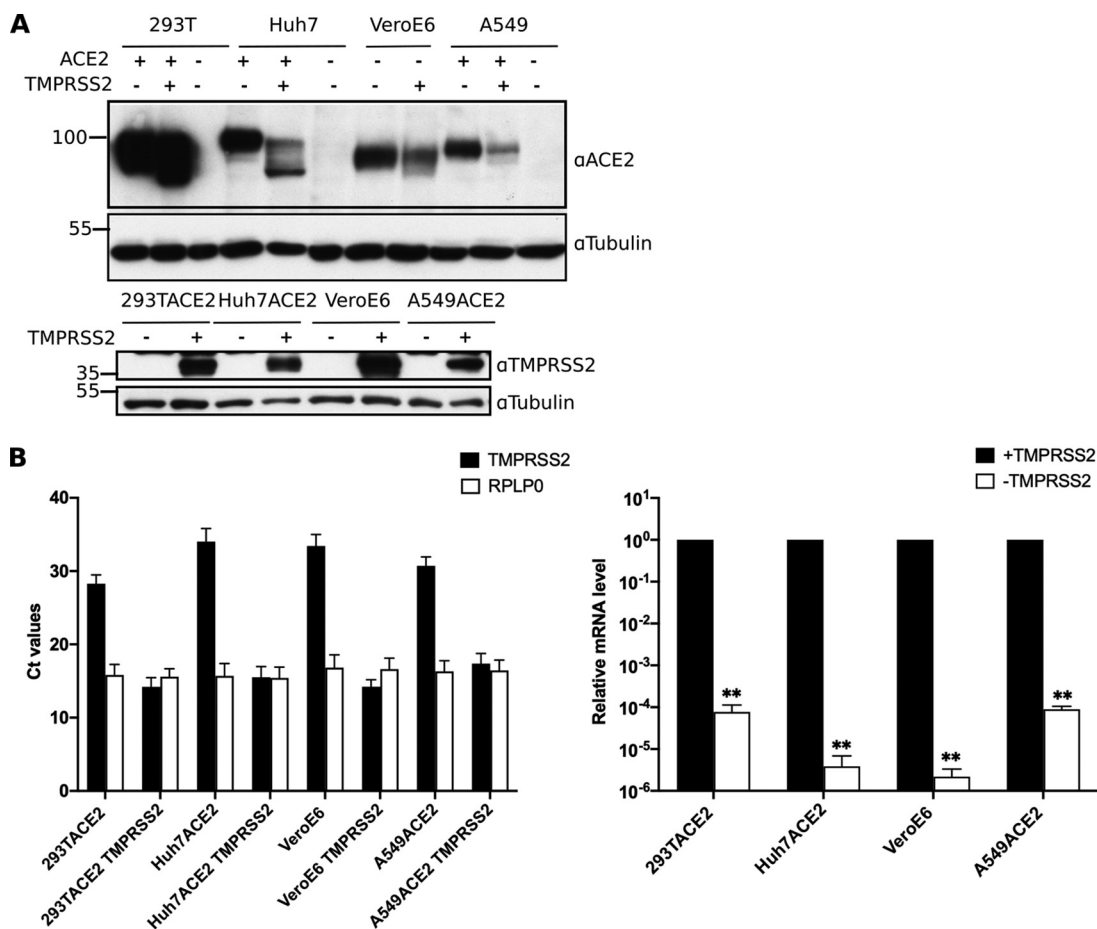


FIG 3 Expression of ACE2 and TMPRSS2 in the different cell lines. (A) The abundance of ACE2 and TMPRSS2 in the lysates of the different cell lines used was determined by Western blotting using ACE2- and TMPRSS2-specific antibodies (α ACE2 and α TMPRSS2). A loading control was done by probing the immunoblots with an anti-tubulin antibody. (B) TMPRSS2 mRNA expression levels in the different cell lines. Bar plots of cycle threshold (C_t) values obtained for the different cell lines in real-time quantitative PCR (RT-qPCR) targeting TMPRSS2 and RPLP0 ribosomal protein housekeeping genes, as well as the expression levels relative to that monitored in the corresponding TMPRSS2-transduced cell line, are shown. **, $P < 0.01$ by Mann-Whitney test.

293T-ACE2, A549-ACE2, Huh7-ACE2, and VeroE6 cells, thus suggesting an entry via the endosomal route in these cells (Fig. 4B). However, in VeroE6 and VeroE6-TMPRSS2 cells, it led to a strong increase in infectivity of control particles pseudotyped with vesicular stomatitis virus glycoprotein (VSV-G), which raised doubts on the specificity of the effect in these cells. To overcome this problem, we determined the effect of the NH_4Cl lysosomotropic agent that blocks the acidification required for endosomal cathepsins activity in the cells. In agreement with the involvement of the endosomal pathway in SARS-CoV-2pp entry, NH_4Cl treatment led to an inhibition of infectivity of Δ fur and Swt particles in all the cells (Fig. 4B). Conversely, camostat mesylate treatment had no effect on infectivity levels in VeroE6, 293T-ACE2, A549-ACE2, and Huh7-ACE2 cells, suggesting that viral pseudoparticles did not use TMPRSS2 serine protease for entering these cells, which is in agreement with the absence of expression of TMPRSS2 in these cells, as shown on the TMPRSS2-specific immunoblot and by the very low level of amplification of TMPRSS2 RNA transcripts in real-time reverse transcription-PCR (Fig. 3A and B). Interestingly, in the four cell lines, Δ fur mutant particles were more sensitive to E64D and NH_4Cl treatment than Swt particles, suggesting that Δ fur mutant particles were more reliant on the endosomal entry pathway than Swt particles. In Huh7-ACE2 cells, pseudoparticles pseudotyped with HCoV-229E that rely on cathepsin activity to enter Huh7 cells (25) were used as positive control of E64D-mediated cathepsin inhibition.

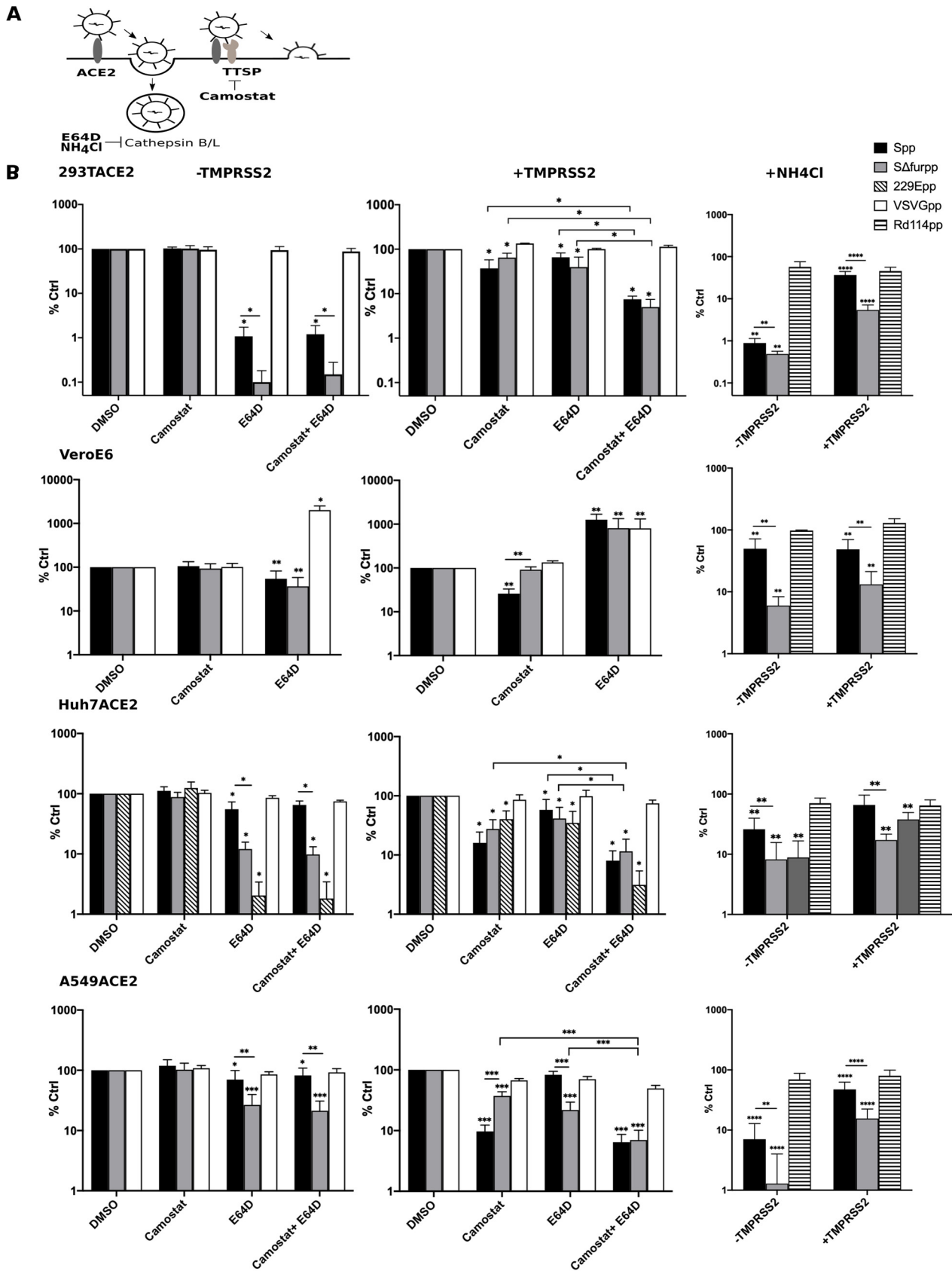


FIG 4 Deletion of spike FCS favors SARS-CoV-2pp endosomal entry in all cell lines. (A) Cartoon illustrating the two routes of entry of coronaviruses, the early pathway involving plasma membrane protease (TMPRSS2) and fusion at the cell surface and the late pathway, during which the virus is (Continued on next page)

As expected, when TMPRSS2 was expressed in 293T-ACE2, VeroE6, A549-ACE2, and Huh7-ACE2 cells, camostat mesylate treatment inhibited Swt pseudoparticles' infectivity. However, the infectivity of the S Δ fur mutant was less affected by inhibition of TMPRSS2 activity than the Swt pseudoparticles. Blockade of the endosomal pathway with E64D still impacted infectivity levels of Swt and S Δ fur mutant viruses in 293T-ACE2-TMPRSS2, Huh7-ACE2-TMPRSS2, and A549-ACE2-TMPRSS2 cells. Moreover, treating the cells with both drugs further reduced the infectivity levels of Swt and, to a higher extent, of S Δ fur mutant viruses. This result indicates that, in these cells, virion entry occurs via both the endosomal and the plasma membrane pathways. Accordingly, NH₄Cl treatment of TMPRSS2-expressing cells strongly inhibited S Δ fur entry (with the highest infectivity level of 17% in A549-ACE2-TMPRSS2 cells; Fig. 3B) while having a mild inhibitory effect on Swt particles' infectivity.

In conclusion, in the different cell types studied, S Δ fur mutant pseudoparticles were more sensitive to inhibition of the endosomal pathway and less sensitive to the inhibition of the early entry pathway than Swt particles. These results suggest that S Δ fur mutant preferentially enters cells via the cathepsin-dependent endosomal pathway.

S2' KR residues and the FCS motif are required for the fusogenic activity of S in VeroE6, 293T-ACE2, and A549-ACE2 cells but are dispensable in Huh7-ACE2 cells.

To further characterize the involvement of the FCS and S2' KR residues in virus propagation, we determined the ability of the FCS and S2' KR mutants to induce syncytium formation in VeroE6, 293T-ACE2, A549-ACE2, and Huh7-ACE2 cells. All the mutants containing FCS mutations were unable to induce the formation of syncytia in VeroE6, A549-ACE2, and 293T-ACE2 cells, whereas the FCS mutation had no dramatic effect in Huh7-ACE2 cells (Fig. 5). Similarly, mutation of the S2' KR residues in the Swt background (S S2') abrogated the ability of S to induce syncytium formation in VeroE6, 293T-ACE2, and A549-ACE2 cells, but not in Huh7-ACE2 cells. However, whereas both FCS and S2' KR mutants could induce syncytium formation in Huh7-ACE2 cells, introduction of KR mutations in the FCS mutant background abrogated the ability of S to induce syncytium formation. We then determined the effect of TMPRSS2 expression on the ability of the different mutants to induce syncytium formation. In VeroE6, 293T-ACE2, and A549-ACE2 cells, TMPRSS2 rescued the formation of syncytia by FCS mutants, whereas no syncytia were observed in cells expressing S mutants harboring KR mutations. Similar to VeroE6, 293T-ACE2, and A549-ACE2 cells, expression of TMPRSS2 in Huh7-ACE2 cells did not rescue the ability of FCS mutants carrying KR mutations to induce syncytia. Furthermore, the absence of basic residues at S1-S2 (S Δ furR685N; Fig. 5) slightly impacted the restoration of syncytium formation upon TMPRSS2 expression in VeroE6, 293T-ACE2, and A549-ACE2 cells.

Thus, the requirement of FCS and basic residues at S2' for S-mediated fusion is cell type dependent. Indeed, S2' KR residues are required for S-induced syncytium formation in VeroE6, 293T-ACE2, and A549-ACE2 cells, whereas they are only required for syncytium formation in the absence of the FCS in Huh7-ACE2 cells. Furthermore, our results confirm that KR residues at S2' are required for TMPRSS2-mediated fusion. Finally, the presence of FCS in SARS-CoV-2 S increases the potential of the S protein to mediate cell-cell fusion in the four cell types.

Requirement of the FCS and S2' KR residues for S processing is host cell dependent. Next, we analyzed the processing of S FCS and S2' KR mutants in the different host cells by Western blotting. While two bands corresponding to the nonprocessed full-length S protein (S0; 180 kDa) and the S1-S2 cleavage product S2 (100 kDa) could be

FIG 4 Legend (Continued)

internalized and spike processed by endosomal cathepsins, leading to fusion between the viral envelope and endosomal membrane. Camostat mesylate inhibits the activity of serine proteases such as TMPRSS2 and, thus, the early pathway, while NH₄Cl and E64D block cathepsin activity and the late pathway. (B) Effect of protease inhibitors on wild-type and FCS mutant SARS-CoV-2pp (Spp and S Δ furpp) entry in different cell types. Cells expressing or not expressing TMPRSS2 were preincubated with or without the different drugs (camostat mesylate, 50 μ M; E64D, 40 μ M; NH₄Cl, 25 mM) for 1 h at 37°C before being infected in the presence of the drug. Forty-eight hours postinfection, cells were lysed, and luciferase activities were quantified. Retroviral MLV pseudoparticles harboring the protein G of the vesicular stomatitis virus (VSVGpp) or the envelope protein of the Rd114 virus (Rd114pp) were used as control. Results are expressed as percentages of infectivity levels relative to that obtained in the absence of drug and are reported as the means \pm standard deviations (error bars) of at least three independent experiments. Statistics were determined by Mann-Whitney with multiple comparisons to no-drug control (*, $P < 0,05$; **, $P < 0,01$; ***, $P < 0,001$; ****, $P < 0,0001$).

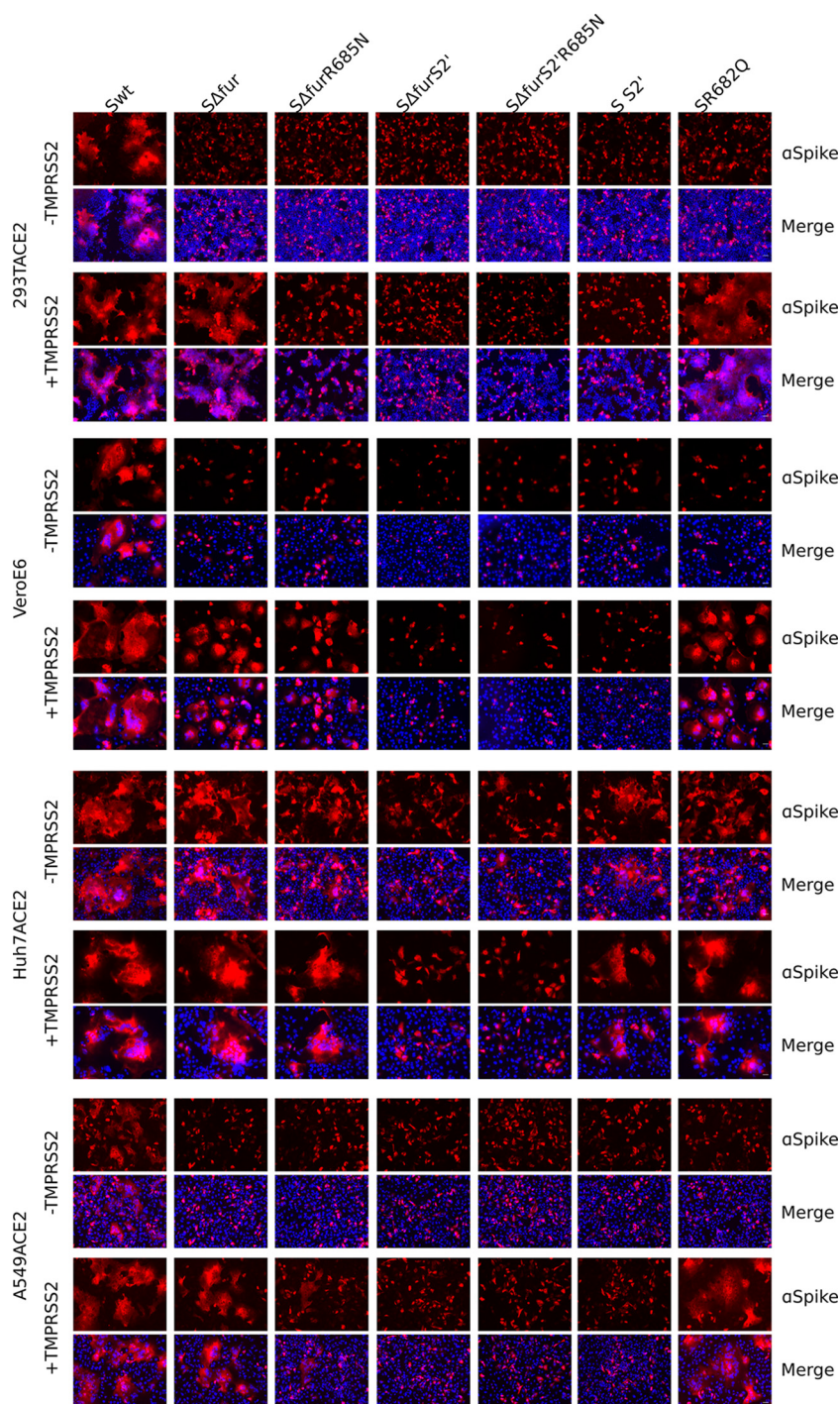


FIG 5 Impact of mutations of FCS and S2' KR residues on the ability of spike to induce syncytium formation. Immunofluorescence staining with DAPI (blue) or an anti-spike antibody (red) of Ver0E6, Huh7-ACE2, A549-ACE2, and 293T-ACE2 cells expressing or not expressing TMPRSS2 and transfected with the wild type (Swt) or mutant S-expressing plasmids (S Δ fur, S Δ furR685N, S Δ furS2', S Δ furS2'R685N, S S2', and S R682Q). Scale bars, 150 μ m.

detected in Swt-expressing cells, only the uncleaved S0 species were detected in 293T-ACE2 and Ver0E6 expressing S mutants (Fig. 6). Furthermore, in A549-ACE2 cells, while no processed product could be detected upon expression of most S mutants, a faint band could be detected at the level of S2 upon S R682Q and S S2' expression. Surprisingly, expression of the FCS mutants in Huh7-ACE2 cells led to the detection of

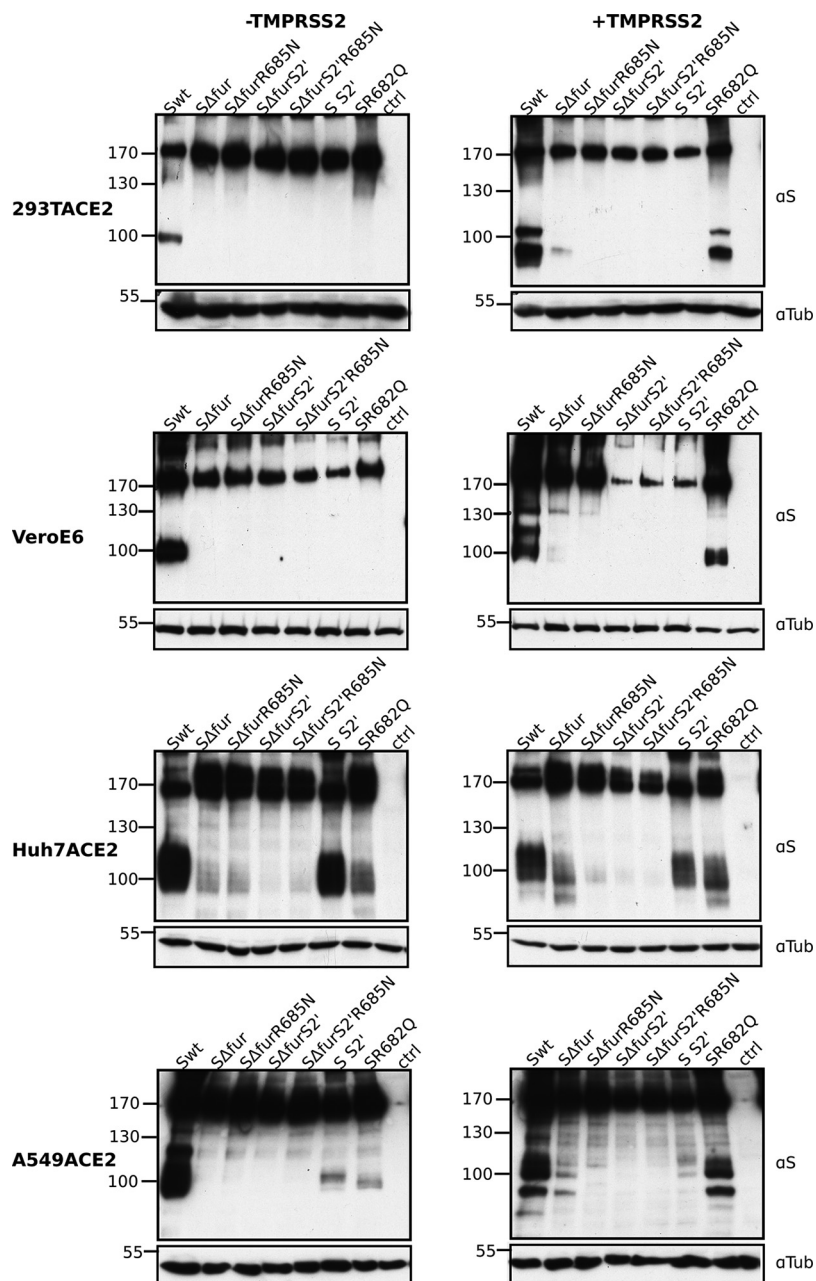


FIG 6 Impact of mutations of FCS and S2' KR residues on the processing of spike. Immunoblots of lysates from VeroE6, 293T-ACE2, Huh7-ACE2, and A549-ACE2 cells expressing or not expressing TMPRSS2 and transfected with wild-type or mutant S-expressing plasmids (SΔfur, SΔfurR685N, SΔfurS2', SΔfurS2'R685N, S S2', and S R682Q). The immunoblots were probed with anti-spike and anti-tubulin MABs.

two bands at the level of the S0 unprocessed product and a band corresponding to the processed product, S2. We have indications that the double band detected around 180 kDa was the result of specific posttranslational modifications of the FCS mutants in Huh7-ACE2 cells (data not shown). In VeroE6, 293T-ACE2, and A549-ACE2 cells, TMPRSS2 expression restored the processing of FCS mutants to different extents depending on the number of basic residues at S1-S2 (more cleavage with the R682Q mutant than with the Δfur mutant) while having no impact on the migration profile of S2' KR mutants (Fig. 6). In Huh7-ACE2 cells, introduction of KR mutations in the SΔfur background seemed to slightly impact the processing of the S protein, while it had no effect on the

processing in the context of Swt. TMPRSS2 expression in Huh7-ACE2 cells did not restore the processing of S Δ furS2' mutants. It is worth noting that the efficiency of the processing of FCS mutants in Huh7-ACE2 cells was quite variable, and, in most assays, only faint bands could be detected at the level of S2 products (Fig. 6 and 7). However, we could still conclude that in most cases, the ability of S mutants to induce syncytia in the host cells correlated with the presence of processed species in the cell lysates.

Finally, the requirement of the FCS and S2' KR residues for S processing and for its ability to induce syncytium formation is cell dependent, and the FCS requirement can only be bypassed by the expression of TMPRSS2. Moreover, S2' KR residues are involved in the processing of S lacking FCS in all studied cell types.

S protein FCS and S2' basic residues mutations affect the accumulation and subcellular localization of S in a cell type-dependent manner. We have seen that, contrary to Swt, FCS and S2' KR mutants were unable to induce the formation of syncytia in VeroE6, 293T-ACE2, and A549-ACE2 cells, while they retained this property in Huh7-ACE2 cells. We hypothesized that these deficiencies could not only be due to a lack of cleavage of spike but also result from an intracellular retention of the mutants. To check it, we characterized the subcellular localization of the different mutants in transfected VeroE6, A549-ACE2, and Huh7-ACE2 cells by immunofluorescence detection using confocal microscopy. As shown in Fig. 8, whereas as observed for the cell surface marker CD4-green fluorescent protein (GFP), Swt located at the plasma membrane of multinucleated cells in VeroE6 and A549-ACE2 cells, FCS, and S2' KR mutants accumulated intracellularly. TMPRSS2 expression rescued the syncytium formation and the cell surface expression of FCS mutants while having no effect on the subcellular localization and syncytium formation of S2' KR mutants. In Huh7-ACE2 cells, only S Δ fur carrying KR mutations (S Δ furS2') seemed to partially localize intracellularly (Fig. 8).

To further determine the ability of the different mutants to reach the cell surface, we analyzed the cell surface expression of S mutants in a biotinylation assay. We used Sulfo-NHS-SS-Biotin to specifically label S proteins present at the plasma membrane. Biotinylated cell surface proteins were subsequently precipitated with streptavidin-conjugated agarose beads. S protein present at the cell surface was then analyzed by Western blotting using an anti-S antibody. Whereas biotinylated uncleaved S0 and processed S2 species could be detected in Swt-expressing VeroE6 and A549-ACE2 cells, no or weaker intensity signals corresponding to S species could be observed for the FCS and S2' KR mutants that accumulated at lower levels than Swt in transfected VeroE6 cells (Fig. 7; S Δ fur, S R682Q, S Δ furR685N, S Δ furS2', S Δ furS2'R685N, and S S2'). Expression of TMPRSS2 increased the level of accumulation of Swt and FCS mutants (S Δ fur, S R682Q, and S Δ furR685N) in the cell lysates as well as their cell surface expression (Fig. 7, "total" and "surface"). However, it had no effect on the expression and cell surface localization of S2' KR mutants (S Δ furS2', S Δ furS2'R685N, and S S2'). Similar results were obtained in 293T-ACE2 cells expressing or not expressing TMPRSS2 (data not shown). These findings suggest that the inability of S2' KR and FCS S mutants to induce syncytium formation in VeroE6, A549-ACE2, and 293T-ACE2 cells might be, at least partly, due to a defect in cell surface expression. In Huh7-ACE2, similar amounts of biotinylated S were detected for FCS and S2' KR mutants and Swt in Western blot analysis, demonstrating that the mutations did not greatly affect the cell surface expression of the S protein (Fig. 7). However, it is worth noting that S Δ furS2' and S Δ furS2'R685N accumulated at slightly lower levels than Swt in transfected Huh7-ACE2 cell lysates, as observed in Fig. 6. Moreover, these mutants seemed to be less efficiently exported at the cell surface in Huh7-ACE2-TMPRSS2 cells, which would be in line with immunofluorescence assay data (Fig. 8). Our data indicate that FCS and S2' KR mutations affect the accumulation and cell surface expression of S in a cell type-dependent manner and that cell surface addressing of FCS mutants can be rescued by TMPRSS2 expression. Taken together, our results suggest that cleavage at S1-S2 is important for cell surface expression of the protein in VeroE6, A549-ACE2, and 293T-ACE2 cells.

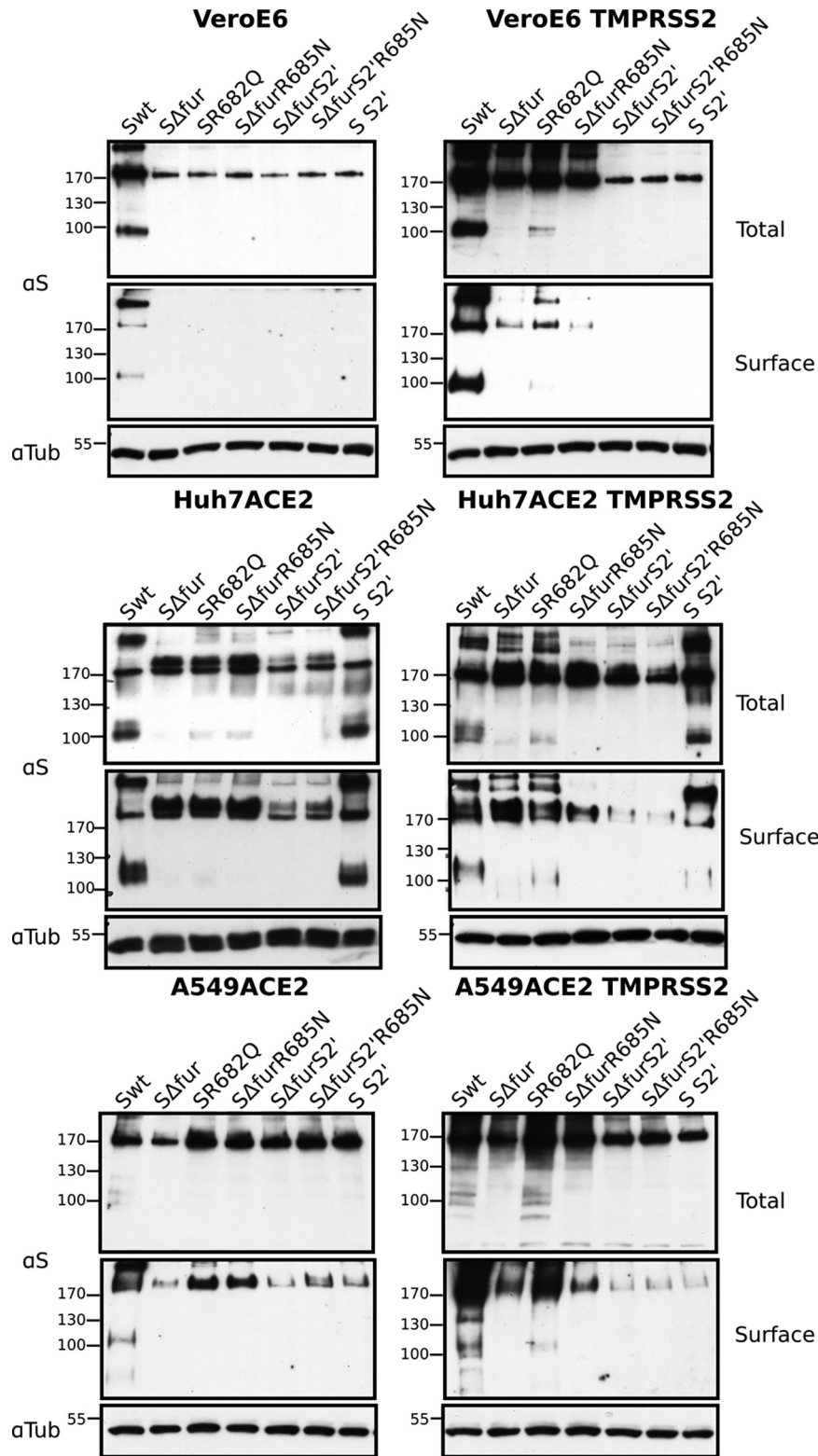


FIG 7 Cell surface biotinylation of spike mutants. Cells expressing wild-type (WT) or mutant (SΔfur, SΔfurR685N, SΔfurS2', SΔfurS2'R685N, S S2', and S R682Q) spike proteins were biotinylated at 4°C and lysed. Cell lysates were analyzed by Western blotting using an anti-spike MAb (total, αS). A loading control was performed by determining the tubulin content of the cell lysates (αTub). Cell-surface biotinylated proteins were precipitated with streptavidin-conjugated agarose beads. Spike abundance in these samples was determined by Western blotting using an anti-spike MAb (surface, αS).

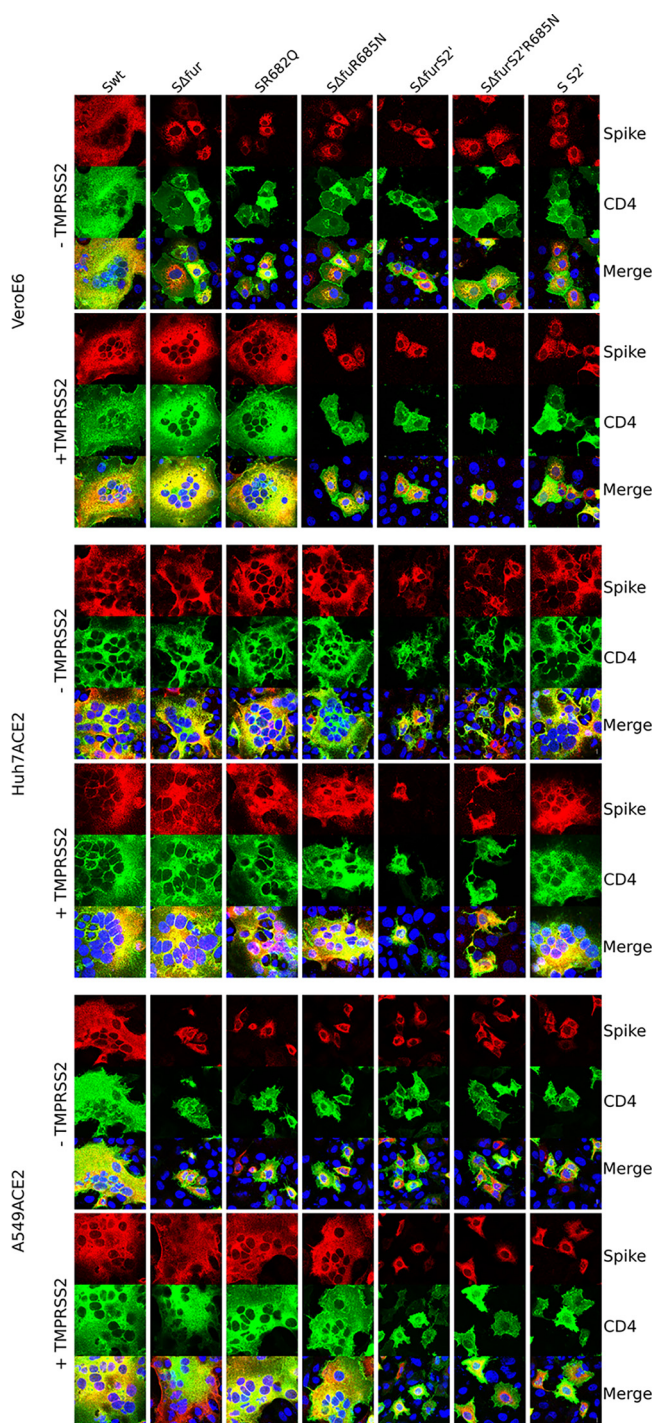


FIG 8 Determination of the subcellular localization of spike mutants by confocal microscopy. VeroE6, Huh7-ACE2, and A549-ACE2 cells expressing or not expressing TMPRSS2 were cotransfected with plasmids encoding the CD4-GFP fusion protein (green) and wild-type (Swt) or mutant spike ($S\Delta fur$, $S\Delta furR685N$, $S\Delta furS2'$, $S\Delta furS2'R685N$, $S S2'$, and $S R682Q$). At 48 h posttransfection, cells were fixed and processed for immunofluorescence detection of spike (red). Nuclei were labeled with DAPI (blue). Scale bars, 10 μm .

The ability of the FCS S mutant to induce cell-to-cell fusion can be rescued by exogenous trypsin. In VeroE6, A549-ACE2, and 293T-ACE2 cells, FCS and $S2'$ KR mutations were found to impact S-mediated syncytium formation, S processing, as well as cell surface expression of the protein. Thus, we sought to determine if the inability of $S\Delta fur$ to induce the formation of syncytia in VeroE6 and A549-ACE2 cells was due to

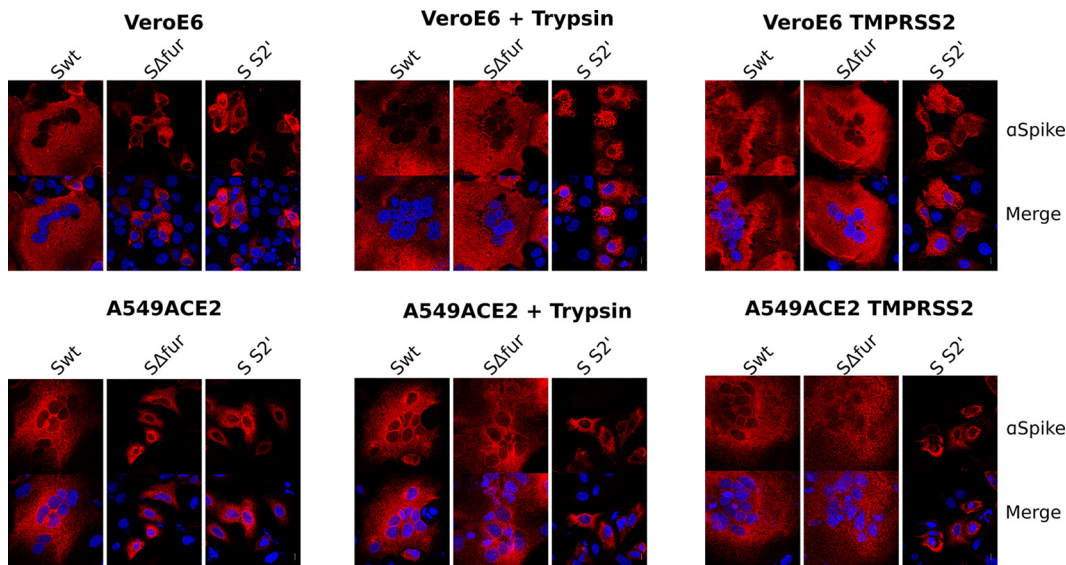


FIG 9 Cell surface activation of spike mutants for fusion by trypsin. Cells expressing wild-type (WT) or mutant ($S\Delta fur$ and $S S2'$) spike proteins were treated with $3 \mu\text{g}/\text{mL}$ trypsin for 40 min and then incubated for 4 h at 37°C in the absence of trypsin and analyzed by immunofluorescence by using an anti-spike antibody (red). Nuclei were labeled with DAPI (blue). Labeled cells were imaged using a confocal microscope. Scale bars, $10 \mu\text{m}$.

the decrease in cell surface expression of the protein or to the lack of processing. For this purpose, we incubated transfected VeroE6 and A549-ACE2 cells with trypsin, which allowed us to specifically cleave spike proteins exposed at the cell surface. As shown in Fig. 9, trypsin treatment rescued the ability of $S\Delta fur$ to induce the formation of syncytia in VeroE6 and A549-ACE2 cells as observed upon TMPRSS2 expression in these cells. In contrast, trypsin treatment had no effect on the inability of $S S2'$ mutant to induce cell-to-cell fusion in both cell lines, as observed in TMPRSS2-expressing cells. Thus, this result indicates that the absence of syncytia in $S\Delta fur$ -expressing VeroE6 and A549-ACE2 cells is, rather, due to a defect in intracellular processing of the protein than to the decreased cell surface expression of S . In addition, the inability of trypsin or TMPRSS2 to activate the $S S2'$ mutant to trigger fusion is in agreement with the importance of $S2'$ KR residues for TMPRSS2-mediated entry.

The furin inhibitor decanoyl-RVKR-chloromethylketone inhibits S-mediated syncytium formation in VeroE6 and A549-ACE2 cells but not in Huh7-ACE2 cells.

Our results suggest that, in specific cellular backgrounds, the ability of S to reach the cell surface and to induce syncytium formation requires a cleavage at the $S1$ - $S2$ FCS. Cell surface expression and formation of syncytia could be prevented either because of the mutation itself that may affect protein folding or because of the inhibition of the furin-mediated protein processing. To further explore these hypotheses, we assessed the effect of the furin/proprotein convertase inhibitor decanoyl-RVKR-chloromethylketone (CMK) on syncytium formation, S processing, and cell surface expression in VeroE6, A549-ACE2, and Huh7-ACE2 cells. As shown in confocal microscopy images (Fig. 10A), CMK treatment inhibited the formation of syncytia in VeroE6 and A549-ACE2 cells expressing S protein, thus resulting in the same phenotype as that observed upon $S\Delta fur$ expression. Conversely, CMK treatment only slightly affected the formation of syncytia in Huh7-ACE2 cells expressing S , which is in agreement with the ability of FCS mutants to induce syncytia in these cells.

While CMK treatment did not affect S localization at the plasma membrane of multinucleated cells in Huh7-ACE2 expressing or not expressing TMPRSS2, we observed an intracellular accumulation of the protein in CMK-treated VeroE6 cells and to a lesser extent in A549-ACE2 cells. TMPRSS2 expression in VeroE6 and A549-ACE2 cells rescued syncytium formation and seemed to increase plasma membrane expression of S . Cell

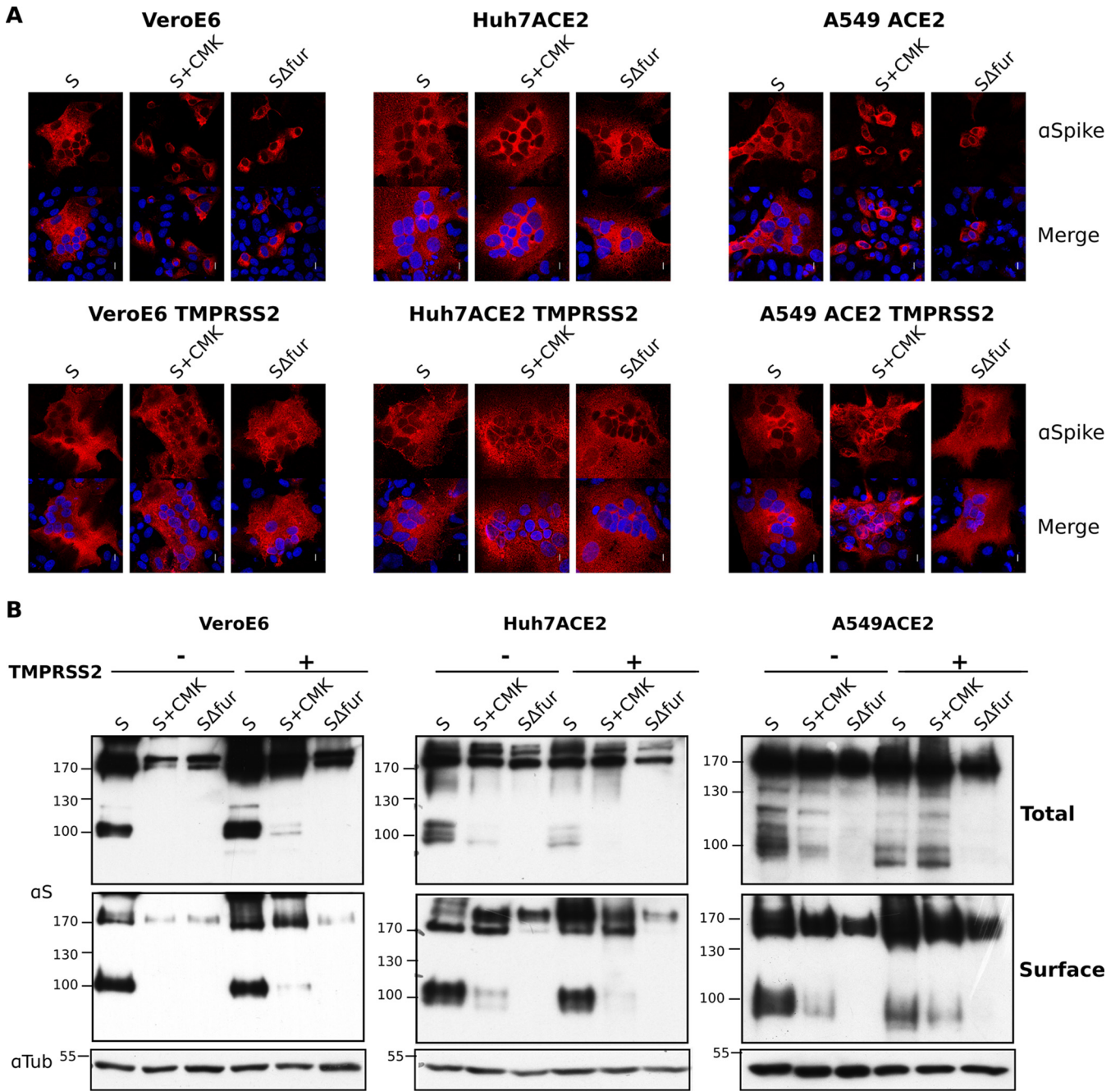


FIG 10 Effect of the CMK furin inhibitor on cell surface expression of spike. (A) Determination of the subcellular localization of spike in CMK-treated cells by confocal microscopy. VeroE6, Huh7-ACE2, and A549-ACE2 cells were transfected or not transfected with TMPRSS2-expressing lentiviral vectors and transfected with plasmids encoding wild-type (Swt) and mutant spike ($S\Delta fur$). Five hours posttransfection, cells were treated or not treated with CMK (50 μM). At 48 h posttransfection, cells were fixed and processed for immunofluorescence detection of spike (red). Nuclei were labeled with DAPI (blue). Scale bars, 10 μm . (B) Cell surface biotinylation of spike in CMK-treated cells. Five hours posttransfection, cells were treated or not treated with CMK (50 μM). At 48 h posttransfection, cells expressing wild-type (WT) or mutant ($S\Delta fur$) spike were biotinylated at 4°C. Spike proteins from the cell lysates were analyzed by Western blotting using an anti-spike MAb (total, αS). A loading control was performed by determining the tubulin content of the cell lysates (αTub). Cell-surface biotinylated proteins were precipitated with streptavidin-conjugated agarose beads. Spike abundance in these samples was determined by Western blotting using an anti-spike MAb (surface, αS).

surface biotinylation experiments revealed that S protein accumulated at lower levels in CMK-treated VeroE6 cells, as observed for $S\Delta fur$ (Fig. 10B, "total"), suggesting that the absence of cleavage affects the stability of the S protein in this cellular background. Additionally, CMK treatment was associated with a decrease in the accumulation of processed S species in the three cell lines (Fig. 10B, "total"). In CMK-treated VeroE6

cells, a lower fraction of the protein reached the cell surface (corresponding to 37% of the proportion of cell surface-expressed S in nontreated cells; Fig. 10B). Conversely, the inhibitor had only a slight effect on the proportion of cell surface-expressed S in A549-ACE2 and Huh7-ACE2 cells (corresponding to 80% of the proportion of cell surface-expressed S in nontreated cells for both cell lines; Fig. 10B). TMPRSS2 expression improved the level of accumulation of S protein, its processing, and cell surface expression in CMK-treated VeroE6 cells (reaching 87% of the proportion of cell surface-expressed S in nontreated cells), as observed for $S\Delta fur$ in VeroE6 cells (Fig. 7 and 10). In CMK-treated A549-ACE2 cells, TMPRSS2 expression led to an increase in the accumulation of processed S species in the cell lysate but had no major impact on the cell surface-expressed S species profile (Fig. 10B, "total" and "surface"). In agreement with the immunofluorescence data, CMK treatment of Huh7-ACE2 and Huh7-ACE2 TMPRSS2 cells did not strongly affect the cell surface expression of S (Fig. 10B).

Thus, these data further support the hypothesis that the inability of $S\Delta fur$ to induce the formation of syncytia in VeroE6 and A549-ACE2 cells is due to a defect in the processing of the protein. Moreover, these results indicate that the induction of syncytium formation by SARS-CoV-2 S in VeroE6 and A549-ACE2 cells involves furin-like proteases and that this requirement can be bypassed by TMPRSS2 expression. In contrast, while S cleavage seems to partially rely on proprotein convertase in Huh7-ACE2 cells, S-induced syncytium formation does not seem to require their activity. In addition, inhibition of furin-like protease activity alters the cell surface expression of the S protein in a cell type-dependent manner, and this defect can be rescued by TMPRSS2 expression.

SARS-CoV-2 infection is inhibited by CMK furin inhibitor in a cell type-dependent manner and can be rescued by TMPRSS2 expression. We then wondered if inhibition of furin-like protease activity would affect SARS-CoV-2 infectivity in a cell type-dependent manner as observed for syncytium formation and cell surface expression. To address this question, we infected VeroE6, A549-ACE2, and Huh7-ACE2 cells expressing or not expressing TMPRSS2 in the presence of CMK. Infectivity levels and S protein processing in the different conditions were assessed by Western blotting using anti-nucleocapsid and anti-spike antibodies, respectively (Fig. 11A). As shown in Fig. 3, we verified that TMPRSS2 was expressed at similar levels in the different transduced cell lines. CMK treatment of Huh7-ACE2 cells drastically inhibited SARS-CoV-2 infection, and S protein expression was hardly detectable in these cells (Fig. 11A and B). Although we observed an inhibition of S processing in CMK-treated VeroE6 and A549-ACE2 cells, infectivity was less affected in these cells, as shown on the anti-N immunoblot (Fig. 11A and B). TMPRSS2 expression strongly increased the infectivity levels and rescued infection in CMK-treated Huh7-ACE2 cells. As shown in Fig. 1, the viral stock used to inoculate the cells mainly harbors uncleaved S proteins at its surface. Our results suggest that in Huh7-ACE2, cleavage by furin-like protease of the S1-S2 boundary is required during entry of the virus.

In parallel, we characterized the syncytial phenotype in each infected host cell line by confocal microscopy by using antispikes immunofluorescence labeling (Fig. 11C). Interestingly, while large syncytia could be observed in infected Huh7-ACE2 cells, no syncytia were observed in VeroE6 cells, in which the S proteins, rather, seemed to accumulate intracellularly. In A549-ACE2 cells, we found an intermediate situation, with S being detected at the surface of syncytia and in intracellular compartments in a fraction of the cell population (Fig. 11C). In these cells, syncytium formation was inhibited by CMK treatment. Expression of TMPRSS2 restored the detection of S in CMK-treated Huh7-ACE2 cells and syncytium formation in CMK-treated Huh7-ACE2 and A549-ACE2 cells (Fig. 11C).

Whereas the weak effect of CMK treatment on VeroE6 and A549-ACE2 infection is in agreement with the fact that the FCS mutation was not detrimental to SARS-CoV-2pp infection, the strong inhibition observed in Huh7-ACE2 cells was quite unexpected. Indeed, in these cells, CMK treatment had no effect on spike-mediated syncytium formation and the FCS mutation did not impact entry of SARS-CoV-2pp.

To further determine which step of SARS-CoV-2 infection was inhibited by CMK, we compared its effect when added during entry, postinoculation, or all the infection

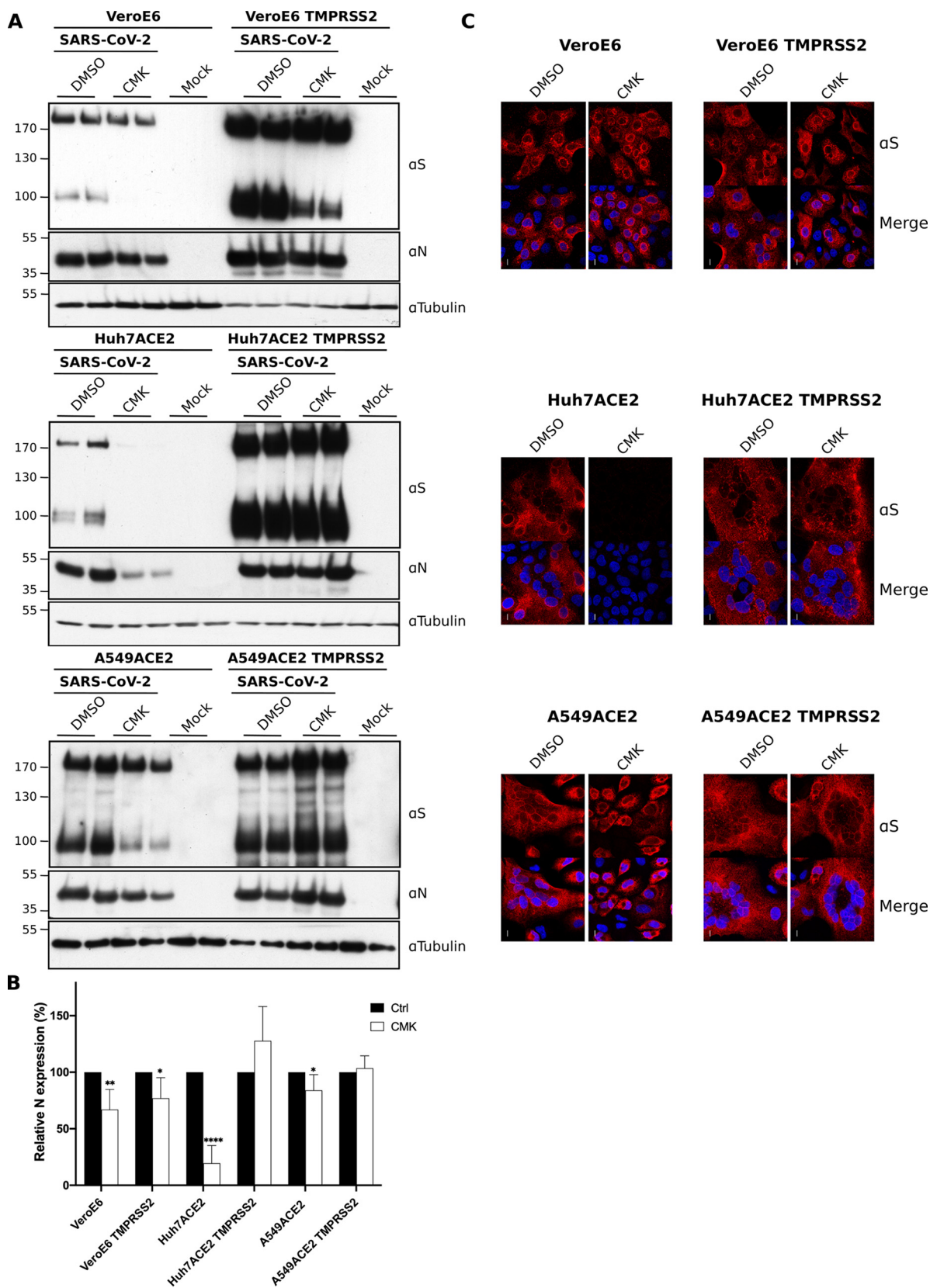


FIG 11 Effect of CMK treatment on SARS-CoV-2 infection in the different host cells. (A) Immunoblot analysis of SARS-CoV-2-infected cells treated or not treated with CMK (50 μ M). VeroE6, Huh7-ACE2, and A549-ACE2 cells expressing or not expressing TMPRSS2 were preincubated for 1 h with CMK (50 μ M) before infection in the presence of the drug. Twenty-four hours postinfection, cells were lysed, (Continued on next page)

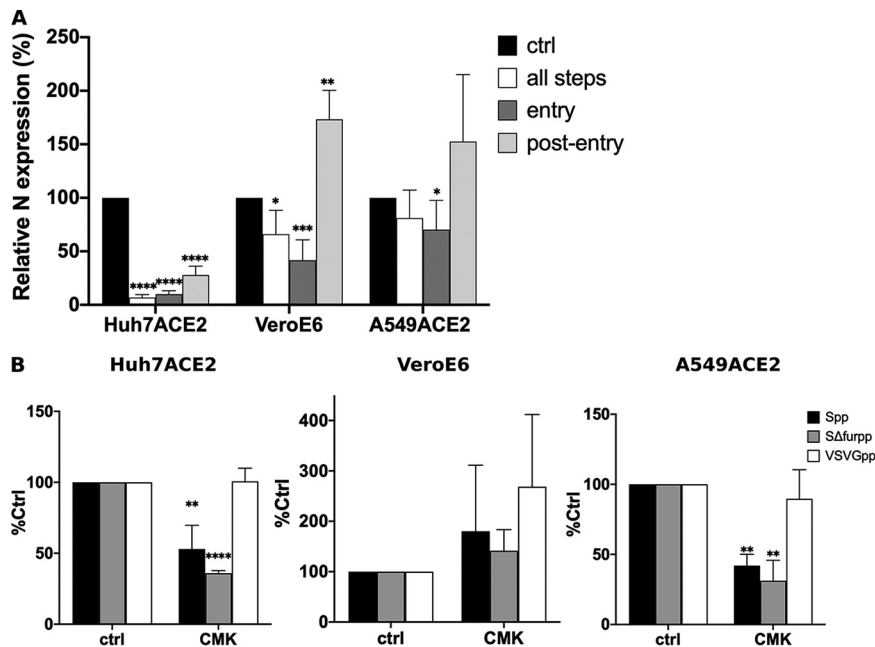


FIG 12 CMK inhibits entry of SARS-CoV-2 in Huh7-ACE2 cells. (A) Time-of-addition experiment. VeroE6, A549-ACE2, and Huh7-ACE2 cells were infected for 1 h with SARS-CoV-2. In the “entry” conditions, CMK was present 1 h before and during the inoculation step as well as 1 h after the removal of the inoculum. In the “postentry” conditions, the drug was added 1 h after the removal of the inoculum and left until the end of the assay. In the “all-steps” conditions, CMK was added 1 h before and during inoculation and left until cell lysis. Twenty-four hours postinfection, the cells were lysed and processed for Western blotting using an anti-nucleocapsid antibody. Graph represents the quantification of the intensity of the band corresponding to the N protein relative to the DMSO control. (B) Effect of CMK on wild-type and FCS mutant SARS-CoV-2pp entry in Huh7-ACE2, A549-ACE2, and VeroE6 cells. Cells were preincubated with CMK (50 μ M) for 1 h at 37°C before being infected in the presence of the drug. Forty-eight hours postinfection, cells were lysed, and luciferase activities were quantified. Retroviral MLV pseudoparticles harboring protein G of the vesicular stomatitis virus (VSVGpp) were used as control. Results are reported as the means \pm standard deviations (error bars) of at least three independent experiments. Statistics were determined by Mann-Whitney test with multiple comparisons to no-drug control (*, $P < 0.05$; **, $P < 0.01$; ***, $P < 0.001$; ****, $P < 0.0001$).

steps (Fig. 12A). In VeroE6 and A549-ACE2 cells, CMK treatment led to 45% and 30% decreases of infectivity level, respectively, when added during the entry step, while it seemed to promote infection when added postentry. In Huh7-ACE2 cells, we observed a strong inhibition (90%) of infection when the drug was added during the entry step and a milder inhibitory effect when it was added postinfection. Thus, these results indicate that CMK inhibits virus entry in Huh7-ACE2 cells. However, the effect observed when the drug is added at the postentry step would require further characterization to draw a conclusion on a potential inhibition of replication or assembly.

In order to further confirm the effect of CMK on the entry step of SARS-CoV-2 infection, we determined its impact on SARS-CoV-2pp infectivity (Fig. 12B). CMK treatment had no significant impact on infectivity levels in VeroE6 cells, whereas it led to a 50% to 60% decrease in infectivity of WT and FCS mutant particles in Huh7-ACE2 cells. We observed a 60% and 70% inhibition of Swt and Δ fur pseudoparticles’ infectivity in CMK-treated A549-ACE2 cells.

FIG 11 Legend (Continued)

and lysates were processed for Western blotting by using nucleocapsid (α N)- or spike (α S)-specific antibodies. Immunoblots were probed with anti-tubulin antibody as loading control (α Tubulin). (B) Graph representing the quantification of the intensity of the band corresponding to the N protein relative to the DMSO control. (C) Immunofluorescence staining and confocal microscopy imaging of SARS-CoV-2-infected cells. Cells infected in the presence or not of CMK (50 μ M) were fixed 24 h postinfection and processed for immunofluorescence detection of spike (red). Nuclei were labeled with DAPI (blue). Scale bars, 10 μ m.

TABLE 1 Summary of the phenotypes of spike mutants

S mutant	Data for VeroE6 cells						Data for Huh7-ACE2 cells					
	-TMPRSS2 ^a			+TMPRSS2			-TMPRSS2			+TMPRSS2		
	Syncytia ^a	Cell surface ^b	Cleavage ^c	Syncytia ^d	Cell surface	Cleavage	Syncytia	Cell surface	Cleavage	Syncytia	Cell surface	Cleavage
WT	+	+	+	+	+	+	+	+	+	+	+	+
Δfur	-	-	-	+	+	+	+	+	+	+	+	+
R682Q	-	-	-	+	+	+	+	+	+	+	+	+
ΔfurR685N	-	-	-	+	+	-	+	+	+	+	+	+
ΔfurS2'	-	-	-	-	-	-	-	+	-	-	+	-
ΔfurS2' R685N	-	-	-	-	-	-	-	+	-	-	+	-
S2'	-	-	-	-	-	-	+	+	+	+	+	+

^aThe ability of spike mutants to induce cell-to-cell fusion in transfected cells was determined by immunofluorescence staining using an anti-spike antibody as shown in Fig. 5 and 7. +, observation of syncytia; -, no syncytia could be observed.

^bCell surface expression of spike mutants was determined by confocal microscopy and by cell surface biotinylation assay as described in Fig. 7 and 8. +, detection of spike at the cell surface; -, decrease in cell surface expression compared to wild-type spike.

^cProcessing of spike mutants was determined by Western blot analysis using an anti-spike antibody as described in Fig. 6. +, presence of cleavage products on the immunoblot, -, no cleavage product detected.

^d+TMPRSS2, with TMPRSS2; -TMPRSS2, without TMPRSS2.

These results further support that SARS-CoV-2 entry in Huh7-ACE2 and A549-ACE2 cells requires furin-like protease activity. However, the fact that CMK inhibits the infectivity of FCS mutant SARS-CoV-2pp suggests that the S protein can be processed at a different site than S1-S2 FCS or, alternatively, that SARS-CoV-2 entry in Huh7-ACE2 cells requires the processing of the host cell factor by furin-like proteases.

Hence, furin-like protease activity is required for SARS-CoV-2 infection in a cell type-dependent manner and can be overcome by TMPRSS2 expression. However, the effect of CMK on the processing and syncytium formation does not necessarily correlate with its impact on SARS-CoV-2 infectivity.

DISCUSSION

The zoonotic potential of coronaviruses might be highly reliant on the variability of the S protein that constitutes the major virus entry determinant. In agreement with the fact that coronavirus entry depends on S proteolytic activation by host cell proteases, variations in and around the spike cleavage sites have been shown to modulate cellular tropism and pathogenesis (26). With SARS-CoV-2 S protein differing from its closest relative by the acquisition of an FCS at the S1-S2 junction, we sought to determine the importance of this feature for S entry functions in different host cells. Moreover, since the fusogenic activity of the S protein requires a second cleavage at the S2' site, we studied the role of conserved basic residues present at the S2' cleavage site in the SARS-CoV-2 S protein. For that purpose, we introduced mutations in these sequences and characterized the phenotypes of these mutants, which are summarized in Table 1. Overall, our data demonstrated that FCS and S2' basic residues modulate S functions in a host cell-dependent manner, most probably reflecting differences in protease expression patterns of the different cell lines (Fig. 13).

The study of the importance of the FCS for S cell-cell fusogenic activity revealed differences according to the cellular expression background (Fig. 13). As observed by others (5, 27), expression of TMPRSS2 allowed bypassing of the requirement of FCS for S to induce syncytia in VeroE6, A549-ACE2, and 293T-ACE2 cells and partly restored S processing. The efficiency of processing rescuing depended on the number of basic residues still present at the S1-S2 junction (compare SΔfur, SΔfurR685N, and S R682Q mutants in Fig. 6). Since TMPRSS2 cleaves at single arginine or lysine residues (monobasic sites), this result supports a cleavage of SARS-CoV-2 S by TMPRSS2 at the S1-S2 site. Furthermore, the detection of two bands at the level of S2 in TMPRSS2-expressing 293T-ACE2 and A549-ACE2 cells suggests that the S protein is cleaved at both S1-S2 and S2' sites in these cells. This situation would be analogous to that found for SARS-CoV spike that has been shown to be cleaved at S1-S2 and activated at S2' by TMPRSS2 (28). However, the fact that S2' KR mutations abrogate the complete processing in TMPRSS2-expressing VeroE6, 293T-ACE2, and A549-ACE2 cells supports a

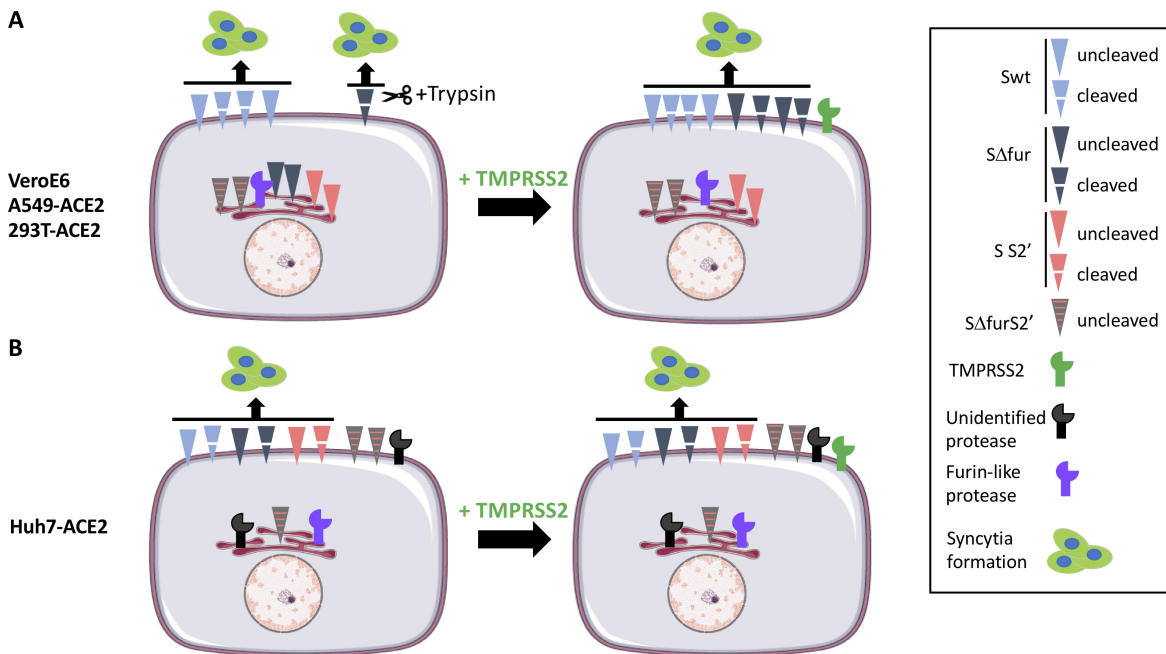


FIG 13 FCS and S2' KR residues modulate S function in a host cell-dependent manner. (A and B) Model depicts the phenotype of FCS and S2' KR S mutants in the different host cells. Expression of S (blue triangles) in all the studied cell lines led to its cell surface expression, its processing, and the formation of syncytia with neighboring cells expressing the ACE2 receptor. Both forms, processed and unprocessed S (cleaved blue triangles and blue triangles, respectively), were detected at the cell surface. When the FCS (gray triangle) or S2' KR residues (pink triangle) were mutated, the impact on the cell surface expression, processing, and ability of the S protein to induce cell-to-cell fusion was dependent on the cellular background. Thus, in VeroE6, 293T-ACE2, and A549-ACE2 cells (A), the mutations led to a partial intracellular retention of the protein, and processing and syncytium formation were abrogated. In these cells, TMPRSS2 expression or exogenous trypsin addition allowed rescue of the ability of the FCS mutant to induce the formation of syncytia. However, expression of this serine protease had no effect on the deficiencies associated with KR mutations. In Huh7-ACE2 cells (B), mutation of FCS or S2' KR had no major impact on syncytium formation, cell surface expression, or processing of the protein. Only mutants carrying FCS and S2' KR mutations (pink-striped, gray triangles) were mainly unprocessed and could not induce the formation of syncytia. TMPRSS2 expression could not rescue these deficiencies.

cleavage at the S2' site only. Alternatively, this result could be due to the fact that S2' KR mutations affect the recognition of the FCS at S1-S2 by furin-like proteases as observed by Barrett et al. (29).

While the priming of coronaviruses S protein at the S1-S2 site is dispensable (30), the S2' cleavage constitutes a critical triggering event since it exposes the internal fusion peptide of the S2 domain at the surface of the virion (31). Moreover, several reports suggest that requirements for spike-mediated activation of cell-cell and virus-cell fusion may differ (1). In our study, TMPRSS2 rescuing of the ability of FCS mutant to induce cell-to-cell fusion is likely to depend on a cleavage of the protein at S2' KR. The fact that mutation of these residues in the FCS background abrogates the rescuing of syncytium formation and processing of the protein supports this hypothesis. This finding suggests that, as found for HCoV-229E and contrary to what has been reported for MERS-CoV S, TMPRSS2 processing of SARS-CoV-2 S at S2' does not require precleavage at S1-S2 (32). In agreement with this, FCS mutations had no impact on SARS-CoV-2 pseudoparticle infectivity in TMPRSS2-expressing cells. This result is not in line with previous studies suggesting that S1-S2 is a prerequisite for subsequent TMPRSS2-mediated activation at the S2' site (5, 33, 34). However, these latter observations are based on experiments performed in the context of infection assays using respiratory cells, such as Calu3 that express low levels of cathepsin, and are thus less efficient in supporting virus entry by the endosomal route. Thus, entry in these cell lines mainly occurs via the early pathway, whereas both pathways were still available in our cellular models. Nevertheless, in our assays (Fig. 4B), TMPRSS2 expression still improved FCS mutant SARS-CoV-2pp infectivity in VeroE6 and A549-ACE2 cells in the presence of the

cathepsin inhibitor E64D, suggesting that FCS was not required for plasma membrane entry in that context (data not shown).

In VeroE6, A549-ACE2, and 293T-ACE2 cellular backgrounds, S2' KR and FCS mutations affected the cell surface expression of S, which could be partially restored upon TMPRSS2 expression in the case of FCS mutants (Fig. 13A). Of note, in our experimental setting, TMPRSS2 was coexpressed with S in the cells. Thus, S cleavage by TMPRSS2 could occur either during intracellular biosynthesis or at the cell surface. As observed upon FCS mutant expression, inhibition of furin-like protease activity by CMK reduced S processing and accumulation, abolished cell-to-cell fusion, and led to an intracellular retention of S in VeroE6 cells. This result suggests that S processing impacts its stability and its subcellular localization (Fig. 10). In a similar manner, the furin-mediated cleavage of the respiratory syncytial virus fusion protein has been shown to be required for its cell surface expression (35). However, in our case, both uncleaved and cleaved spike species could be detected at the cell surface (Fig. 7 and 10).

Although FCS mutations impacted the cell surface expression of S in VeroE6 and A549-ACE2, enough proteins were available at the cell surface to trigger fusion with neighboring cells upon trypsin activation (Fig. 9 and Fig. 13A). This result is in agreement with the fact that a very low number of fusion proteins is required to induce fusion. Indeed, in the case of the type I influenza fusion glycoprotein, hemagglutinin (HA), it has been estimated that fusion requires the concerted action of at least three HA trimers (36).

Surprisingly, FCS and S2' KR mutations had no or reduced impact on S processing, cell surface expression, and syncytium formation in Huh7-ACE2 cells (Fig. 13B). Nevertheless, it is worth noting that we observed some interexperimental variations in the level of accumulation of processed S species for the mutants carrying FCS mutations in Huh7-ACE2 cells. Since FCS mutations can affect the accumulation and trafficking of S in some cellular backgrounds, they might impact these processes with milder intensity in Huh7 cells and thus affect the accessibility of the protein to specific proteases. In agreement with this hypothesis, some of our data suggest that FCS mutations affect S posttranslational modifications and the kinetics of S processing (data not shown). Thus, the suboptimal proteolysis of the FCS mutant might be more impacted by experimental variability. The heterogeneity in proteolytic processing of FCS mutants could also be related to variability of protease expression profiles in Huh7 cells. However, further experiments would be required to better characterize the parameters that impact S processing in Huh7 cells. Mutations of both FCS and S2' KR cleavage sites led to defects in processing and syncytium formation in these cells. These findings illustrate that acquisition of FCS by S increases its fusogenic potential since either FCS or S2' KR is required for spike to induce fusion in Huh7-ACE2 cells, while S2' KR residues are absolutely required for spike to induce fusion in VeroE6, A549-ACE2, and 293T-ACE2 cells. While the processing of S2' KR FCS mutants in Huh7-ACE2 cells seemed to be suppressed, these mutations barely affected cell surface expression of the protein (Fig. 7). The lower impact of cleavage site mutations on S processing and ability to induce cell-to-cell fusion in Huh7-ACE2 cells compared to other tested cell lines suggests that they express specific proteases that can process and activate S for fusion at distinct sequences. Therefore, in our model of cell-cell fusion, FCS and S2' KR mutants are expressed at the cell surface and processed, expression of TMPRSS2 has no major effect on cell-cell fusion, and basic residues either at S1-S2 or at S2' can activate cell-cell fusion (Fig. 13B). In agreement with this hypothesis, SARS-CoV-2 S protein seems to be processed by a wide range of proteases (37). Thus, several other serine proteases than TMPRSS2 (TMPRSS4, TMPRSS11a, TMPRSS11d, and TMPRSS11e) (7) have been shown to enhance S-mediated cell-cell fusion, but their ability to activate S for infection has not been characterized yet. More recently, Nguyen and collaborators (29) reported that matrix metalloproteases were involved in cell-cell fusion but not in SARS-CoV-2 pseudoparticle infection.

Importantly, confocal microscopy observations revealed different patterns of expression for the S protein in the different infected cell lines. Indeed, only few syncytia could be observed in infected VeroE6 cells where S mainly localizes intracellularly. In contrast,

the S protein was mainly associated with syncytia in Huh7-ACE2 cells, and an intermediate situation was found in A549-ACE2 cells in which S was found to be both associated with syncytia and in intracellular compartments. Intracellular accumulation of S in infected VeroE6 cells is in agreement with the results of Boson et al. showing that the SARS-CoV-2 E protein was inducing the intracellular retention of S by slowing down the secretory pathway (38). However, cell surface expression of S in infected Huh7-ACE2 and A549-ACE2 cells suggests that E-mediated intracellular retention of S is cell type specific. Furthermore, observation of large syncytia in Huh7-ACE2 cells is in agreement with the expression of specific S-targeting proteases in these cells. This is supported by the high fraction of processed S species in the lysates of infected Huh7-ACE2 cells (Fig. 11A). These differences in syncytial phenotypes suggest that virus propagation mechanisms might highly depend on the host cell. Thus, in Huh7-ACE2 cells, infection might rely on both extracellular, as well as cell-to-cell, virus transmission, whereas the later route might be less important in VeroE6 cells (39).

Interestingly, mutation of FCS likely affects the entry route used by the virus. Thus, our results suggest that FCS mutants prefer the endosomal entry pathway and therefore are more sensitive to NH_4Cl and E64D treatments. Interestingly, in SARS-CoV-2 infection assays, viral entry was inhibited by CMK treatment, as previously observed (40) in VeroE6 cells. However, in all the tested cell lines, we observed a difference of sensitivity to protease inhibitors of authentic SARS-CoV-2 particles from SARS-CoV-2 pseudoparticles (Fig. 12). This might be due to the fact that pseudoparticles that are produced in 293T cells mainly harbor cleaved spike proteins, while SARS-CoV-2 authentic particles produced in VeroE6 cells are mainly decorated with uncleaved spike proteins (as shown in Fig. 1).

In Huh7-ACE2 cells, the strong inhibition of SARS-CoV-2 entry by CMK was in agreement with the impact of the treatment on the infectivity of pseudoparticles. However, the fact that CMK inhibited WT as well as FCS mutant particles' infectivity suggests that furin-like proteases can process the S protein at a site other than S1-S2 or, alternatively, that entry requires the processing of host cell factors by furin-like proteases. Interestingly, computational analysis of the spike sequence allowed the identification of several amino acid sequences in different regions of spike susceptible to cleavage by furin (35). Of note, the MERS-CoV spike protein has been reported to contain two furin cleavage sites at S1-S2 and S2' sites that have been reported to mediate furin activation for entry into the host cell (41). However, Matsuyama et al. later observed that inhibition of MERS-CoV infection by CMK could also result from an effect on TMPRSS2 and cathepsin L (42). These findings indicate that CMK can have limited specificity, being able to inhibit cathepsin, TMPRSS2, trypsin, and papain in certain conditions (43). In our study, the effect of CMK treatment on S-expressing cells correlated with FCS mutant phenotypes, thus allowing us to attribute the observed phenotypes to furin-like protease activity defects (Fig. 10). However, the effect observed in the different infected cell lines might be attributed to inhibition of other proteases than furin. Of note, TMPRSS2 rescuing of infection in Huh7-ACE2 cells would be in agreement with an effect of CMK on the endosomal entry pathway, which would be in line with inhibition of cathepsins or other proprotein convertases present in endosomes and not in favor of an effect on TMPRSS2.

Overall, our study allowed us to better characterize the importance of FCS and S2' KR sequences for spike entry function. Importantly, it highlights the high heterogeneity in the S sequence requirement for entry functions in different host cells, thus illustrating the high adaptability of the SARS-CoV-2 virus to its host environment.

MATERIALS AND METHODS

Construction of SARS-CoV-2 spike mutants. The human codon-optimized sequence of the SARS-CoV-2 spike protein (GenBank accession number [MN908947](#)) was cloned in the pcDNA3.1(+) vector with a sequence coding for the HA tag in the C terminus. Spike protein mutants were generated by fusion PCR using the external primers SARS2-FW 5'-TCAAAGCTTGCCACCATGTTCTGTCTTCTGGTCT-3' and SARS2-REV 5'-TCGGATCC GGTGTAGTGCGACTTCACGC-3' and internal primers carrying sequence substitutions.

Cell culture. Human HEK293T/17 cells (ATCC), Huh7, simian VeroE6 cells (Sigma-Aldrich; a gift from Caroline Goujon), and A549 human lung carcinoma cells (ATCC CCL-185) were cultured in Dulbecco's modified eagle medium (DMEM) (Life Technologies) supplemented with 10% fetal bovine serum, 2 mM GlutaMax, and nonessential amino acids (Life Technologies). Absence of mycoplasma contamination was regularly checked in the cell cultures. A549 stably expressing ACE2 cells were used for SARS-CoV-2 infection assays and were kindly provided by Delphine Muriaux.

Antibodies and drugs. Mouse anti-SARS-CoV-2 spike S2 antibody was obtained from Euromedex, SARS-CoV-2 nucleocapsid was detected using a rabbit polyclonal antibody (Novus), human TMPRSS2 was detected with a rabbit monoclonal antibody from Abcam (catalog no. ab92323), and mouse anti-tubulin was from Sigma. Anti-capsid of murine leukemia virus (MLV; ATCC CRL1912) was produced *in vitro* by using a MiniPerm apparatus (Heraeus) as recommended by the manufacturer.

E64D (2S,3S)-trans-Epoxy succinyl-L-leucylamido-3-methylbutane ethyl ester was purchased from Merck, and camostat mesylate was purchased from Sigma. Decanoyl-RVCR-chloromethylketone (CMK; furin convertase inhibitor) was from Enzo Life Science.

Plasmid transfection. Cells were seeded in 24-well plates or 12-well plates and transfected with 250 ng or 500 ng of plasmid DNA using Trans-IT LT1 transfection reagent (Mirus Bio) or TurboFect (Thermo Scientific) according to the manufacturer's instructions. Further analyses were performed 48 h posttransfection.

Spike-pseudotyped retroviral particles production and infection. Retroviral particles pseudotyped with the S glycoprotein of the SARS-CoV-2 (SARS-CoV-2pp) were produced as previously reported by Millet and Whittaker (44) with plasmids encoding WT or mutant SARS-CoV-2 spike proteins at 33°C. Supernatants containing the pseudotyped particles were harvested 72 h posttransfection, filtered through 0.45- μ m-pore-size membranes to be used in infection assays or pelleted by ultracentrifugation through a 20% sucrose cushion at 27,000 rpm (Beckman type SW41 rotor) for 4 h at 4°C, and analyzed by Western blotting using an anti-SARS-CoV-2 spike S2 antibody or an anti-murine leukemia virus capsid (ATCC CRL1912) antibody. To minimize artifacts that might be caused by differences in quality of preparation, each experiment was performed using concurrently produced pseudoparticles. Cells transduced or not transduced with lentiviral vectors expressing ACE2 or TMPRSS2 for 72 h were infected with SARS-CoV-2pp in 48-well dishes. Firefly luciferase activities were quantified 72 h postinfection as indicated by the manufacturer (Promega).

Virus production and cell infection. SARS-CoV-2 (isolate hCoV-19_IPL_France; GenBank accession number MW575140) was propagated on VeroE6 cells expressing TMPRSS2 as previously described (45).

For infection in the presence of CMK, cells were preincubated with CMK 50 μ M for 1 h and infected in the presence of the drug or dimethyl sulfoxide (DMSO) for 24 h. Cells were then fixed or lysed and processed for immunofluorescence or Western blotting, respectively.

Lentivirus production and transduction. To produce lentivirus stocks, HEK293T/17 cells were seeded in 6-well dishes. The next day, cells were transfected with 500 ng pTRIP vector expressing ACE2 or TMPRSS2, 400 ng of HIV gag-pol-expressing vector, and 100 ng of vesicular stomatitis virus G protein-expressing vector with TurboFect according to the manufacturer's instructions. Virus stocks were collected 48 h posttransfection and filtered. Cells were transduced by incubation with lentivirus-containing supernatants between 48 and 72 h at 37°C. For experiments of pseudotyped particle infection in the presence of protease inhibitors, populations of Huh7, 293T-ACE2, and A549 cells stably expressing TMPRSS2 were generated by selecting transduced cells with puromycin.

Immunofluorescence. For immunofluorescence microscopy, cells were grown on glass coverslips and fixed with 3% paraformaldehyde (PFA; Sigma-Aldrich) for 20 min. The cells were permeabilized for 3 min in phosphate-buffered saline (PBS) and 0.1% Triton X-100. Cells were then incubated in 10% goat serum-PBS blocking buffer for 10 min. Both primary and secondary antibody incubations were carried out in blocking buffer for 30 min at room temperature. Nuclei were stained by a 5-min incubation in PBS containing 1 μ g/mL DAPI (4',6-diamidino-2-phenylindole). Coverslips were mounted on glass slides using Mowiol 4-88-based mounting medium. Images were acquired using an inverted laser scanning confocal microscope (LSM 880; Zeiss), using a 63 \times (1.4 numerical aperture) oil immersion lens.

Western blotting. Cells were rinsed with cold PBS and lysed at 4°C for 20 min in PBS lysis buffer (1% Triton X-100 and a mixture of protease inhibitors [Roche]). Insoluble material was removed by centrifugation at 4°C. Protein samples were heated for 7 min at 70°C in Laemmli sample buffer and resolved by SDS-PAGE. The proteins were then transferred onto nitrocellulose membranes (Hybond-ECL; Amersham) using a Trans-Blot apparatus (Bio-Rad). Proteins of interest were revealed upon incubation of the membrane with specific primary antibodies followed by incubation with species-specific secondary antibodies conjugated to peroxidase. Detection of proteins was done using enhanced chemiluminescence (ECL Plus; GE Healthcare). Quantification of unsaturated signals was carried out using the gel quantification function of ImageJ.

Quantification of mRNA. Total RNA was isolated from cells using the kit NucleoSpin RNA Plus (Macherey-Nagel) followed by cDNA synthesis using high-capacity cDNA reverse transcription kit (Applied Biosystems). The expression levels of specific mRNA were determined by quantitative real-time PCR (qPCR) using TaqMan gene expression assays (Life Technologies).

Cell surface biotinylation. Cells were seeded in 6-well plates and transfected the next day with WT or mutant spike-expressing plasmids. Twenty-four to 48 h posttransfection, cells were rinsed with cold PBS and incubated 30 min at 4°C with 0.3 mg/mL EZ-Link Sulfo-NHS-SS-Biotin (Pierce) in PBS to label cell surface proteins. Unreacted biotin was quenched with 50 mM glycine in PBS buffer. Cells were then rinsed with cold PBS and lysed with B1 buffer (50 mM Tris, pH 7.5, 100 mM NaCl, 2 mM EDTA, 1% Triton X-100, 0.1% SDS, and protease inhibitor mixture) on ice. Lysates were centrifuged at 14,000 rpm at 4°C

to remove cellular debris, and biotinylated proteins were recovered using streptavidin-agarose beads (Amersham Biosciences). After washing, the bound proteins were detected by immunoblotting.

Graphs and statistics. Prism version 5.0c software (GraphPad Software, Inc., La Jolla, CA) was used for creating graphs and to determine statistical significance of differences between data sets by using Mann-Whitney tests.

ACKNOWLEDGMENTS

We thank P. Charneau for providing 293T-ACE2 cells and Delphine Muriaux for providing A549-ACE2 cells. We thank Lowiese Desmarts for her diligent proofreading. The immunofluorescence analyses were performed with the help of the imaging core facility of the Biomedicine Center Lille Nord-de-France.

Conceived and designed experiments, M.L. and S.B.; performed experiments, M.L. and S.B.; provided reagents, M.L. and S.B.; analyzed the data, M.L. and S.B.; and wrote the paper, M.L., S.B., and J.D.

REFERENCES

- Tang T, Bidon M, Jaimes JA, Whittaker GR, Daniel S. 2020. Coronavirus membrane fusion mechanism offers a potential target for antiviral development. *Antiviral Res* 178:104792. <https://doi.org/10.1016/j.antiviral.2020.104792>.
- Dessie G, Malik T. 2021. Role of serine proteases and host cell receptors involved in proteolytic activation, entry of SARS-CoV-2 and its current therapeutic options. *Infect Drug Resist* 14:1883–1892. <https://doi.org/10.2147/IDR.S308176>.
- Gioia M, Ciaccio C, Calligaris P, De Simone G, Sbardella D, Tundo G, Fasciglione GF, Di Masi A, Di Pierro D, Bocedi A, Ascenzi P, Coletta M. 2020. Role of proteolytic enzymes in the COVID-19 infection and promising therapeutic approaches. *Biochem Pharmacol* 182:114225. <https://doi.org/10.1016/j.bcp.2020.114225>.
- Hoffmann M, Kleine-Weber H, Schroeder S, Krüger N, Herrler T, Erichsen S, Schiergens TS, Herrler G, Wu N-H, Nitsche A, Müller MA, Drosten C, Pöhlmann S. 2020. SARS-CoV-2 cell entry depends on ACE2 and TMPRSS2 and is blocked by a clinically proven protease inhibitor. *Cell* 181:271–280. <https://doi.org/10.1016/j.cell.2020.02.052>.
- Hoffmann M, Kleine-Weber H, Pöhlmann S. 2020. A multibasic cleavage site in the spike protein of SARS-CoV-2 is essential for infection of human lung cells. *Mol Cell* 78:779–784. <https://doi.org/10.1016/j.molcel.2020.04.022>.
- Buchrieser J, Duffoo J, Hubert M, Monel B, Planas D, Rajah MM, Planchais C, Porrot F, Guivel-Benhassine F, Van der Werf S, Casartelli N, Mouquet H, Bruel T, Schwartz O. 2020. Syncytia formation by SARS-CoV-2-infected cells. *EMBO J* 40:e107405. <https://doi.org/10.15252/embj.2020107405>.
- Ou X, Liu Y, Lei X, Li P, Mi D, Ren L, Guo L, Guo R, Chen T, Hu J, Xiang Z, Mu Z, Chen X, Chen J, Hu K, Jin Q, Wang J, Qian Z. 2020. Characterization of spike glycoprotein of SARS-CoV-2 on virus entry and its immune cross-reactivity with SARS-CoV. *Nat Commun* 11:1620. <https://doi.org/10.1038/s41467-020-15562-9>.
- Bussani R, Schneider E, Zentilin L, Collesi C, Ali H, Braga L, Volpe MC, Colliva A, Zanonati F, Berlot G, Silvestri F, Zacchigna S, Giacca M. 2020. Persistence of viral RNA, pneumocyte syncytia and thrombosis are hallmarks of advanced COVID-19 pathology. *EBioMedicine* 61:103104. <https://doi.org/10.1016/j.ebiom.2020.103104>.
- Stadlmann S, Hein-Kuhnt R, Singer G. 2020. Viroplasmic multinuclear syncytial giant cells in bronchial fluid from a patient with COVID-19. *J Clin Pathol* 73:607–608. <https://doi.org/10.1136/jclinpath-2020-206657>.
- Tian S, Hu W, Niu L, Liu H, Xu H, Xiao S-Y. 2020. Pulmonary pathology of early-phase 2019 novel coronavirus (COVID-19) pneumonia in two patients with lung cancer. *J Thorac Oncol* 15:700–704. <https://doi.org/10.1016/j.jtho.2020.02.010>.
- Xu Z, Shi L, Wang Y, Zhang J, Huang L, Zhang C, Liu S, Zhao P, Liu H, Zhu L, Tai Y, Bai C, Gao T, Song J, Xia P, Dong J, Zhao J, Wang F-S. 2020. Pathological findings of COVID-19 associated with acute respiratory distress syndrome. *Lancet Respir Med* 8:420–422. [https://doi.org/10.1016/S2213-2600\(20\)30076-X](https://doi.org/10.1016/S2213-2600(20)30076-X).
- Peacock TP, Goldhill DH, Zhou J, Baillon L, Frise R, Swann OC, Kugathasan R, Penn R, Brown JC, Sanchez-David RY, Braga L, Williamson MK, Hassard JA, Staller E, Hanley B, Osborn M, Giacca M, Davidson AD, Matthews DA, Barclay WS. 2021. The furin cleavage site in the SARS-CoV-2 spike protein is required for transmission in ferrets. *Nat Microbiol* 6:899–909. <https://doi.org/10.1038/s41564-021-00908-w>.
- Johnson BA, Xie X, Kalveram B, Lokugamage KG, Muruato A, Zou J, Zhang X, Juelich T, Smith JK, Zhang L, Bopp N, Schindewolf C, Vu M, Vanderheiden A, Swetnam D, Plante JA, Aguilar P, Plante KS, Lee B, Weaver SC, Suthar MS, Routh AL, Ren P, Ku Z, An Z, Debbink K, Shi PY, Freiberg AN, Menachery VD. 2020. Furin cleavage site is key to SARS-CoV-2 pathogenesis. *BioRxiv*. <https://doi.org/10.1101/2020.08.26.268854>.
- Ogando NS, Dalebout TJ, Zevenhoven-Dobbe JC, Limpens RWAL, van der Meer Y, Caly L, Druce J, de Vries JJC, Kikkert M, Bárcena M, Sidorov I, Snijder EJ. 2020. SARS-coronavirus-2 replication in VeroE6 cells: replication kinetics, rapid adaptation and cytopathology. *J Gen Virol* 101:925–940. <https://doi.org/10.1099/jgv.0.001453>.
- Liu Z, Zheng H, Lin H, Li M, Yuan R, Peng J, Xiong Q, Sun J, Li B, Wu J, Yi L, Peng X, Zhang H, Zhang W, Hulswit RJG, Loman N, Rambaut A, Ke C, Bowden TA, Pybus OG, Lu J. 2020. Identification of common deletions in the spike protein of severe acute respiratory syndrome coronavirus 2. *J Virol* 94:e00790-20. <https://doi.org/10.1128/JVI.00790-20>.
- Wong YC, Lau SY, Wang To KK, Mok BWY, Li X, Wang P, Deng S, Woo KF, Du Z, Li C, Zhou J, Chan JFW, Yuen KY, Chen H, Chen Z. 2021. Natural transmission of bat-like severe acute respiratory syndrome coronavirus 2 without proline-arginine-alanine variants in coronavirus disease 2019 patients. *Clin Infect Dis* 73:e437–e444. <https://doi.org/10.1093/cid/cia953>.
- Klimstra WB, Tilston-Lunel NL, Nambulli S, Boslett J, McMillen CM, Gilliland T, Dunn MD, Sun C, Wheeler SE, Wells A, Hartman AL, McElroy AK, Reed DS, Rennick LJ, Duprex WP. 2020. SARS-CoV-2 growth, furin-cleavage-site adaptation and neutralization using serum from acutely infected hospitalized COVID-19 patients. *J Gen Virol* 101:1156–1169. <https://doi.org/10.1099/jgv.0.001481>.
- Davidson AD, Williamson MK, Lewis S, Shoemark D, Carroll MW, Heesom KJ, Zambon M, Ellis J, Lewis PA, Hiscox JA, Matthews DA. 2020. Characterisation of the transcriptome and proteome of SARS-CoV-2 reveals a cell passage induced in-frame deletion of the furin-like cleavage site from the spike glycoprotein. *Genome Med* 12:e68. <https://doi.org/10.1186/s13073-020-00763-0>.
- Sasaki M, Uemura K, Sato A, Toba S, Sanaki T, Maenaka K, Hall WW, Orba Y, Sawa H. 2021. SARS-CoV-2 variants with mutations at the S1-S2 cleavage site are generated in vitro during propagation in TMPRSS2-deficient cells. *PLoS Pathog* 17:e1009233. <https://doi.org/10.1371/journal.ppat.1009233>.
- Walls AC, Park Y-J, Tortorici MA, Wall A, McGuire AT, Veerles D. 2020. Structure, function, and antigenicity of the SARS-CoV-2 spike glycoprotein. *Cell* 181:281–292. <https://doi.org/10.1016/j.cell.2020.02.058>.
- Johnson BA, Xie X, Bailey AL, Kalveram B, Lokugamage KG, Muruato A, Zou J, Zhang X, Juelich T, Smith JK, Zhang L, Bopp N, Schindewolf C, Vu M, Vanderheiden A, Winkler ES, Swetnam D, Plante JA, Aguilar P, Plante KS, Popov V, Lee B, Weaver SC, Suthar MS, Routh AL, Ren P, Ku Z, An Z, Debbink K, Diamond MS, Shi P-Y, Freiberg AN, Menachery VD. 2021. Loss of furin cleavage site attenuates SARS-CoV-2 pathogenesis. *Nature* 591:293–299. <https://doi.org/10.1038/s41586-021-03237-4>.
- Belouzard S, Chu VC, Whittaker GR. 2009. Activation of the SARS coronavirus spike protein via sequential proteolytic cleavage at two distinct sites. *Proc Natl Acad Sci U S A* 106:5871–5876. <https://doi.org/10.1073/pnas.0809524106>.
- Heurich A, Hofmann-Winkler H, Gierer S, Liepold T, Jahn O, Pöhlmann S. 2014. TMPRSS2 and ADAM17 cleave ACE2 differentially and only proteolysis by TMPRSS2 augments entry driven by the severe acute respiratory

- syndrome coronavirus spike protein. *J Virol* 88:1293–1307. <https://doi.org/10.1128/JVI.02202-13>.
24. Kawase M, Shirato K, van der Hoek L, Taguchi F, Matsuyama S. 2012. Simultaneous treatment of human bronchial epithelial cells with serine and cysteine protease inhibitors prevents severe acute respiratory syndrome coronavirus entry. *J Virol* 86:6537–6545. <https://doi.org/10.1128/JVI.00094-12>.
 25. Kawase M, Shirato K, Matsuyama S, Taguchi F. 2009. Protease-mediated entry via the endosome of human coronavirus 229E. *J Virol* 83:712–721. <https://doi.org/10.1128/JVI.01933-08>.
 26. Coutard B, Valle C, de Lamballerie X, Canard B, Seidah NG, Decroly E. 2020. The spike glycoprotein of the new coronavirus 2019-nCoV contains a furin-like cleavage site absent in CoV of the same clade. *Antiviral Res* 176:104742. <https://doi.org/10.1016/j.antiviral.2020.104742>.
 27. Zhu Y, Feng F, Hu G, Wang Y, Yu Y, Zhu Y, Xu W, Cai X, Sun Z, Han W, Ye R, Qu D, Ding Q, Huang X, Chen H, Xu W, Xie Y, Cai Q, Yuan Z, Zhang R. 2021. A genome-wide CRISPR screen identifies host factors that regulate SARS-CoV-2 entry. *Nature* 12:961. <https://doi.org/10.1038/s41467-021-21213-4>.
 28. Reinke LM, Spiegel M, Plegge T, Hartleib A, Nehlmeier I, Gierer S, Hoffmann M, Hofmann-Winkler H, Winkler M, Pöhlmann S. 2017. Different residues in the SARS-CoV spike protein determine cleavage and activation by the host cell protease TMPRSS2. *PLoS One* 12:e0179177. <https://doi.org/10.1371/journal.pone.0179177>.
 29. Nguyen HT, Zhang S, Wang Q, Anang S, Wang J, Ding H, Kappes JC, Sodroski J. 2021. Spike glycoprotein and host cell determinants of SARS-CoV-2 entry and cytopathic effects. *J Virol* 95:23. <https://doi.org/10.1128/JVI.02304-20>.
 30. Heald-Sargent T, Gallagher T. 2012. Ready, set, fuse! The coronavirus spike protein and acquisition of fusion competence. *Viruses* 4:557–580. <https://doi.org/10.3390/v4040557>.
 31. Whittaker GR, Daniel S, Millet JK. 2021. Coronavirus entry: how we arrived at SARS-CoV-2. *Curr Opin Virol* 47:113–120. <https://doi.org/10.1016/j.coviro.2021.02.006>.
 32. Bonnin A, Danneels A, Dubuisson J, Goffard A, Belouzard S. 2018. HCoV-229E spike protein fusion activation by trypsin-like serine proteases is mediated by proteolytic processing in the S2' region. *J Gen Virol* 99:908–912. <https://doi.org/10.1099/jgv.0.001074>.
 33. Papa G, Mallery DL, Albecka A, Welch L, Cattin-Ortolá J, Luptak J, Paul D, McMahon HT, Goodfellow IG, Carter A, Munro S, James LC. 2021. Furin cleavage of SARS-CoV-2 spike promotes but is not essential for infection and cell-cell fusion. *PLoS Pathog* 17:e1009246. <https://doi.org/10.1371/journal.ppat.1009246>.
 34. Tang T, Jaimes JA, Bidon MK, Straus MR, Daniel S, Whittaker GR. 2021. Proteolytic activation of SARS-CoV-2 spike at the S1-S2 boundary: potential role of proteases beyond furin. *ACS Infect Dis* 7:264–272. <https://doi.org/10.1021/acscinfdis.0c00701>.
 35. Bolt G, Pedersen LØ, Birkeslund HH. 2000. Cleavage of the respiratory syncytial virus fusion protein is required for its surface expression: role of furin. *Virus Res* 68:25–33. [https://doi.org/10.1016/s0168-1702\(00\)00149-0](https://doi.org/10.1016/s0168-1702(00)00149-0).
 36. Lenard J. 1999. Viral membranes, p 1920–1925. *In* Granoff A, Webster R (ed), *Encyclopedia of virology*. Elsevier, Academic Press, Cambridge, MA.
 37. Jaimes JA, Millet JK, Whittaker GR. 2020. Proteolytic cleavage of the SARS-CoV-2 spike protein and the role of the novel S1-S2 site. *iScience* 23:101212. <https://doi.org/10.1016/j.isci.2020.101212>.
 38. Bosen B, Legros V, Zhou B, Siret E, Mathieu C, Cosset F-L, Lavillette D, Denolly S. 2021. The SARS-CoV-2 envelope and membrane proteins modulate maturation and retention of the spike protein, allowing assembly of virus-like particles. *J Biol Chem* 296:100111. <https://doi.org/10.1074/jbc.RA120.016175>.
 39. Zeng C, Evans JP, King T, Zheng Y-M, Oltz EM, Whelan SPJ, Saif L, Peeples ME, Liu S-L. 2021. SARS-CoV-2 spreads through cell-to-cell transmission. *Proc Natl Acad Sci U S A* 119:e2111400119. <https://doi.org/10.1073/pnas.2111400119>.
 40. Cheng Y-W, Chao T-L, Li C-L, Chiu M-F, Kao H-C, Wang S-H, Pang Y-H, Lin C-H, Tsai Y-M, Lee W-H, Tao M-H, Ho T-C, Wu P-Y, Jang L-T, Chen P-J, Chang S-Y, Yeh S-H. 2020. Furin inhibitors block SARS-CoV-2 spike protein cleavage to suppress virus production and cytopathic effects. *Cell Rep* 33:108254. <https://doi.org/10.1016/j.celrep.2020.108254>.
 41. Millet JK, Whittaker GR. 2014. Host cell entry of Middle East respiratory syndrome coronavirus after two-step, furin-mediated activation of the spike protein. *Proc Natl Acad Sci U S A* 111:15214–15219. <https://doi.org/10.1073/pnas.1407087111>.
 42. Matsuyama S, Shirato K, Kawase M, Terada Y, Kawachi K, Fukushi S, Kamitani W. 2018. Middle East respiratory syndrome coronavirus spike protein is not activated directly by cellular furin during viral entry into target cells. *J Virol* 92:e00683-18. <https://doi.org/10.1128/JVI.00683-18>.
 43. Pišlar A, Mitrović A, Sabotić J, Pečar Fonović U, Perišić Nanut M, Jakoš T, Senjor E, Kos J. 2020. The role of cysteine peptidases in coronavirus cell entry and replication: the therapeutic potential of cathepsin inhibitors. *PLoS Pathog* 16:e1009013. <https://doi.org/10.1371/journal.ppat.1009013>.
 44. Millet J, Whittaker G. 2016. Murine leukemia virus (MLV)-based coronavirus spike-pseudotyped particle production and infection. *Bio Protoc* 6:e2035. <https://doi.org/10.21769/BioProtoc.2035>.
 45. Belouzard S, Machelart A, Sencio V, Vausselin T, Hoffmann E, Deboosere N, Rouillé Y, Desmarests L, Séron K, Danneels A, Robil C, Belloy L, Moreau C, Piveteau C, Biela A, Vandeputte A, Heumel S, Deruyter L, Dumont J, Leroux F, Engelmann I, Alidjinou EK, Hober D, Brodin P, Beghyn T, Trottein F, Déprez B, Dubuisson J. 2022. Clofoctol inhibits SARS-CoV-2 replication and reduces lung pathology in mice. *PLoS Pathog* 18:e1010498. <https://doi.org/10.1101/2021.06.30.450483>.